DISCLAIMER:

This document does not meet the
current format guidelines of
the Graduate School at
The University of Texas at Austin.

It has been published for
informational use only.

The Thesis Committee for Gabriel Giacomone
Certifies that this is the approved version of the following Thesis

ENHANCING THE MODEL OF COARSE-GRAINED BASIN FLOOR FANS; CHARACTERISTIC TRENDS WITHIN LOBES AND LOBE COMPLEXES OF THE JURASSIC LOS MOLLES FM., NEUQUEN BASIN, ARGENTINA

APPROVED BY
SUPERVISING COMMITTEE:

Ronald j. Steel, Supervisor

Cornel Olariu, Co-Supervisor

Zoltan Sylvester

ENHANCING THE MODEL OF COARSE-GRAINED BASIN FLOOR FANS; CHARACTERISTIC TRENDS WITHIN LOBES AND LOBE COMPLEXES OF THE JURASSIC LOS MOLLES FM., NEUQUEN BASIN, ARGENTINA

by

Gabriel Giacomone

Thesis

Presented to the Faculty of the Graduate School of

The University of Texas at Austin

in Partial Fulfillment

of the Requirements

for the Degree of

Master of Science in Geological Sciences

The University of Texas at Austin

May 2019

Dedication

To all beloved members of the Giacomone family, to my partner in life Flavia and all my Argentinean friends who supported me throughout my stay in the United States

Acknowledgements

Thank you to my supervisors, Ron Steel and Cornel Olariu for allowing me to be part of the amazing team of Dynamic Stratigraphy at UT. I am very grateful to have met Dr Ron Steel on a course in Buenos Aires; since then we have had many discussions and I feel today I would not be the geologist I am if I had not met him. Thank you, Cornel, for always pushing me to doubt everything and pursue new and creative ideas; your advice either on the field or at the office were immensely helpful for me to achieve this degree. Thank you, Zoltan Sylvester, for all the good discussions in one of the best courses I have attended at UT, Sediment Gravity-Flow Depositional Systems. This class was very helpful and applicable to my research and future career.

Special thanks to my field assistants, Gonzalo Fernandez and my good friend and colleague Alejandro Gomez Dacal, for all the hard but fun work on the field. Your insights and experience in sedimentology were very valuable. Thank you to the rest of Neuquen Basin group; Yuqian Gan, Flavio Almeida, Eunsil Jung and Moonsoo Shin, having you around on the field and sharing thoughts on our area made it easier for me to understand our geological context. Thank you to all the Dynamic Stratigraphy group for the great weekly meetings we have had this last 2 years, were so many great and crazy ideas were discussed.

I am grateful to have had the support of our sponsors (YPF, Pluspetrol S.A., and Shell) and the Jackson School of Geosciences, who provided essential funds for my research. A special mention to the Fulbright program whose sponsorship made it possible for me to pursue a graduate degree at UT.

Thank you to all the people in Alumine, Argentina for always being so welcoming. Thank you, Nestor, for being the perfect host and preparing the best *asados*. Thank you, Cordero, Bagley, Rambeau and Beymalec estancias for letting me walk around and explore their land.

Lastly, I would like to thank my good friends, family, and girlfriend. Thank you, Esteban, Gabo, Ian, Ruso, Ema, Richard, Betty, Lucia, Lean and Pao; you all made it easy for me to be living on a foreign country and you are the reason I could call Austin a home.

To my parents Delfor and Graciela, and my brothers and sisters Javier, Andres and Mariel, thank you for all your unconditional support and love. Each one of you was an example for me to follow and become who I am today.

Finally, thank you to my girlfriend and partner in life Flavia Petean. You inspire me every day to be a better person and scientist; your support and love are a source of calmness to my anxious personality.

Abstract

ENHANCING THE MODEL OF COARSE-GRAINED BASIN FLOOR FANS; CHARACTERISTIC TRENDS WITHIN LOBES AND LOBE COMPLEXES OF THE JURASSIC LOS MOLLES FM., NEUQUEN BASIN, ARGENTINA

Gabriel Giacomone, MS Geo Sci

The University of Texas at Austin, 2019

Supervisors: Ron Steel and Cornel Olariu

Basin floor fans can contain a wide range of grain sizes, though the most frequently described fans have tended to be the fine-grained sandy and muddier ones. A coarse-grained category of fan has been broadly described previously, but it lacks a depositional and facies model. The Mid-Jurassic deep-water marine deposits of Los Molles Fm. in Neuquén Basin, Argentina is an example of this type of fan and it is well exposed in outcrop. A detailed characterization of the basin-floor fans of La Jardinera is used to build a coarse-grained fan model.

We made use of a high-resolution satellite image, drone imagery and 4000 m of logs with detailed measurements to build isopach and net/gross (NG) maps that with facies analysis allowed reconstruction of the fan and its lobe complexes (LC1-5). In addition, grain size, facies and bed thickness trends were used to refine the interpretation at a lobe scale within unit LC3. Lithofacies, NG ratios and sandstone body geometry helped define six facies associations; hemipelagic deposits, lobe fringe, off-axis lobes, on-axis lobes, distributary channels and debris flows. The facies associations build lobes (<10 m thick) and these are grouped into lobe complexes (~20-40 m thick). The studied five lobe complexes (LC1-5) are separated by fine-grained intervals (~ 4 m thick in average). The fan shows paleoflow

trends towards the northwest at the bottom gradually changing to northeast at the top. The lobe complexes stack forward and backstep gently, with no major switches; they aggrade and shift laterally in an autocyclic manner, following topographic lows left by previous deposits. The maps at lobe complex scale show an overall elongated morphology and serrated geometries downdip, a normal response of focused sediment dispersal associated with channels and high-density turbidity currents. Detailed study of lobes 3 and 4 in LC3 show that proximal to lobe axis beds are thicker (>40 cm), grain size is greater (medium sand to granules) and main facies are conglomerates and structureless sandstones. Off axis, beds are thinner (<40 cm), grain size ranges from fine to medium sand and there is an increase on normally graded and laminated sands. These trends are associated with the confinement and density of the flow. From lobe axis to off-axis, channelized elements disappear and the facies vary from high density to low density turbidites.

The present work shows a coarse-grained basin floor fan system that differs from previous models; having a distinct elongated morphology, finger-like geometries and changes in facies associated with channelized features and variations on the type of flow from the axis to the fringes.

Table of Contents

List of Tables

List of Figures

1. Introduction

The basin floor fan deposits were thought to be dominated by muds mainly deposited as pelagic sediments. (Maury, 1855 *apud* Mutti *et al.*, 2009) but the improved bathymetry techniques allowed the recognition of deposits at the base of continental slope and lead to the proposition of the deep-water fan model (Menard, 1955; William R. Normark (2), 1978; Normark *et al.*, 1979; Mutti & Normark, 1987). Coarse-grained, deep- water fan models have been proposed and developed along with the turbidity current paradigm and the development of sequence-stratigraphy (Mutti, 1985). However, the proposed coarse-grained deep-water model focuses mainly on the overall large-scale morphology of the fan (William R. Normark (2), 1978; Normark *et al.*, 1979, 2006; Piper & Normark, 1983; Bowen *et al.*, 1984; Kenyon *et al.*, 2002; Pichevin *et al.*, 2003; Gervais *et al.*, 2004, 2006b; a; Deptuck *et al.*, 2008). On the other hand, studies that focused on facies analysis were made on outcrops that are not very extensive, thus larger scale features might be missing (Link & Nilsen, 1980; Cazzola *et al.*, 1985; Sinclair, 1994; Joseph *et al.*, 2000; Satur *et al.*, 2000; Camacho *et al.*, 2002; Felletti, 2016). The outstanding and extensive outcrops of early-mid Jurassic Los Molles Fm. in Neuquén Basin, Argentina present the chance to refine the model for coarse-grained deep-water fans.

The evolution of basin-floor fans and how they are formed in terms of their complex geometric assemblage from bed scale features (individual flow events) to large-scale lobe stacking and lobe complexes has received much attention (e.g. Prélat *et al.*, 2009; Mulder & Etienne, 2010; Prélat & Hodgson, 2013, Grundvåg *et al.*, 2014). Architectural and hierarchical analysis has been made mainly on fine-grained sandy and muddy deposits (e.g. Permian Karoo basin, Prélat *et al.*, 2009; Eocene Central Basin of Spitsbergen, Grundvåg *et al.*, 2014), and has yet to be refined for coarse grained systems.

Several authors have studied the Los Molles Fm. outcrops in Neuquén Basin. Some have focused on large-scale stratigraphy (Burgess *et al.*, 2000; Paim *et al.*, 2008, 2011; Vann *et al.*, 2014; Olariu *et al.*, 2019 in press); others in gravity flow processes (Mutti *et al.*, 2003), though some focused on facies variability and local architecture within specific intervals of the basin floor fans (Tudor, 2014; Shin, 2015).

In this study we (1) propose a 3D model for the coarse-grained fans by using the details of facies and architecture analysis of the Los Molles deposits combined with other literature examples, (2) increase our understanding of the Los Molles basin-floor deposits in the context of

the shelf-slope-basin floor clinoform physiography of the Neuquén Basin and possible topographic influence on the fans, and (3) provide reservoir analogs for the subsurface since Cuyo Group (slope-basin floor Los Molles, shelf deposits of Lajas and fluvial deposits of Challaco Fms.) contain significant hydrocarbon resources.

2. Geological Setting

The Neuquén basin is located in central western Argentina and Eastern Chile, between 32° and 41° latitude (Fig. 1). It encompasses the provinces of Neuquén, Mendoza, Rio Negro and La Pampa. The basin has a triangular shape, covers approximately 120000 km^2 (Yrigoyen, 1991) and comprises a record from the Late Triassic to Early Cenozoic that exceeds 7000 m of marine and continental stratigraphy (Ramos, 1998).

The basin is generally divided in two main regions: Neuquén Andes to the west, and Neuquén embayment to the east (Howell *et al.*, 2005). It is bordered by the Andean chain to the west and two cratons to the east: The Sierra Pintada system to the northeast and north Patagonian Massif to the southeast (Fig. 1).

This study is located in the area called "Arroyo La Jardinera", on the southwest margin of Neuquén basin, southeast to the city of Alumine (Fig. 1 and 2). The outcrops in the area show extensive deposits of Cuyo Group (Los Molles Fm., Lajas Fm. and Challaco Fm.) that allow great documentation to be obtained at different scales of work.

The evolution and development of Neuquén Basin have been summarized in three main stages (Fig. 3; Gustavo D. Vergani, Anthony J. Tank, 1995; Franzese *et al.*, 2003; Howell *et al.*, 2005; Olariu *et al.*, 2019 in press). The first stage occurs from Late Triassic to Early Jurassic (Rift phase); the western part of Argentina and eastern Chile underwent extensional tectonic processes associated to an arc system along the western margin of Gondwana (Paim *et al.*, 2008, Legarreta & Uliana, 1991, Gulisano and Gutierrez Pleimling 1994). This led to a series of narrow, isolated depressions filled with continental facies and volcanic materials with great lateral thickness variation known as Precuyo Group (Gulisano & Gutierrez Pleimling, 1994). The second stage occurs from Early Jurassic to Early Cretaceous where there was a back arc setting with regional subsidence, associated with the development of a steeply dipping, active subduction zone (Howell *et al.*, 2005). The third and last stage spans from Late Cretaceous to Cenozoic times; the subduction

zone shallowed, resulting in a classic foreland basin associated with compression and flexural subsidence (Ramos 1998).

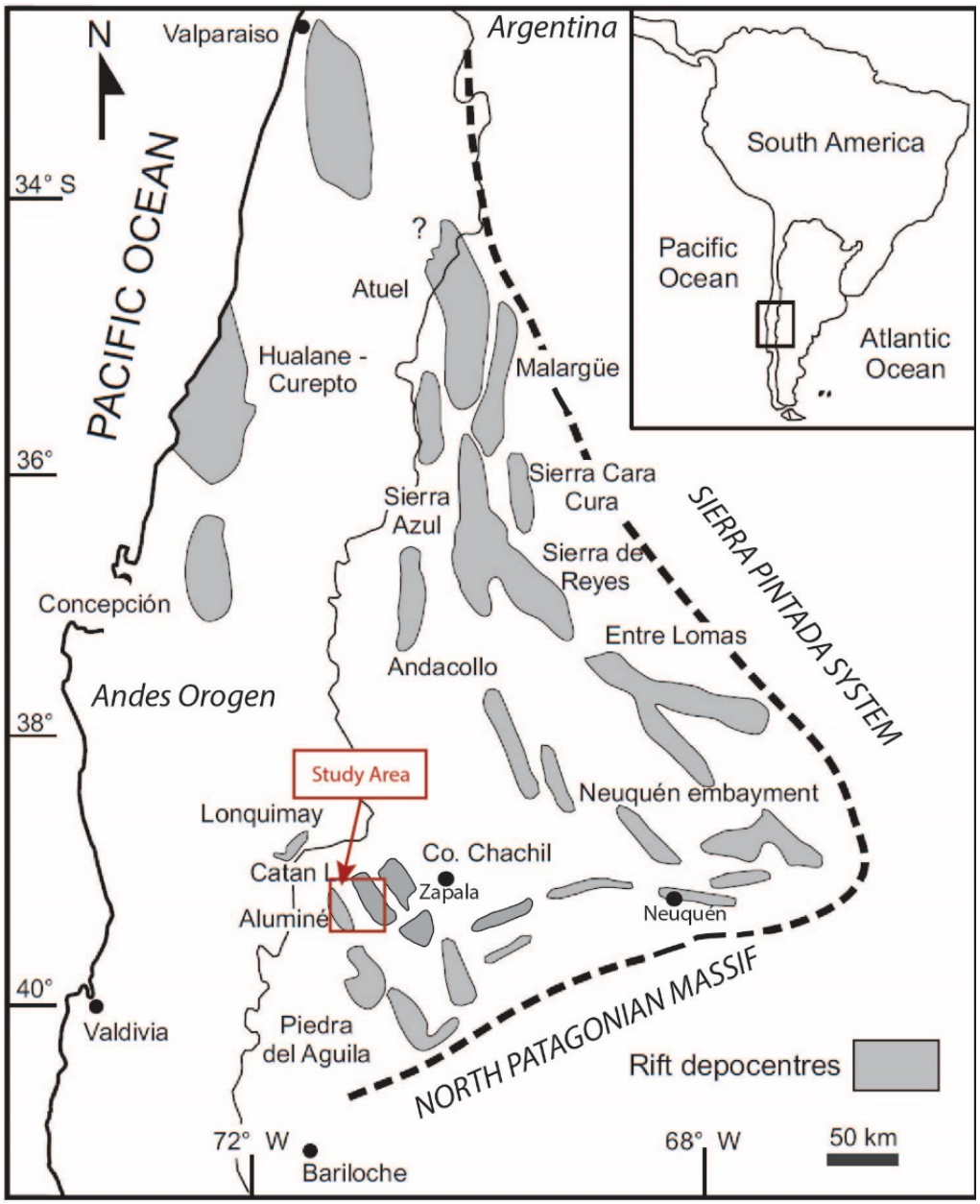

Figure 1. Regional map of Neuquén basin with rift depocenters distribution and location of the study area. Modified from Franzese & Spalletti, 2001.

The Los Molles Fm. has a variable total thickness, with maximum values of 2,000 m in the Huincul high area (Omil *et al.*, 2002). The age for the entire interval is Pliensbachian – Early Bajocian, varying with the position within the basin (Arregui *et al.*, 2011). This study will focus on the lowermost part of this succession (Pliensbachian – Early Toarcian), represented by

approximately 150 - 200 m of medium to coarse-grained sandstones and conglomerates that built a basin floor fan that sits on top of Pleinsbachian dark shale.

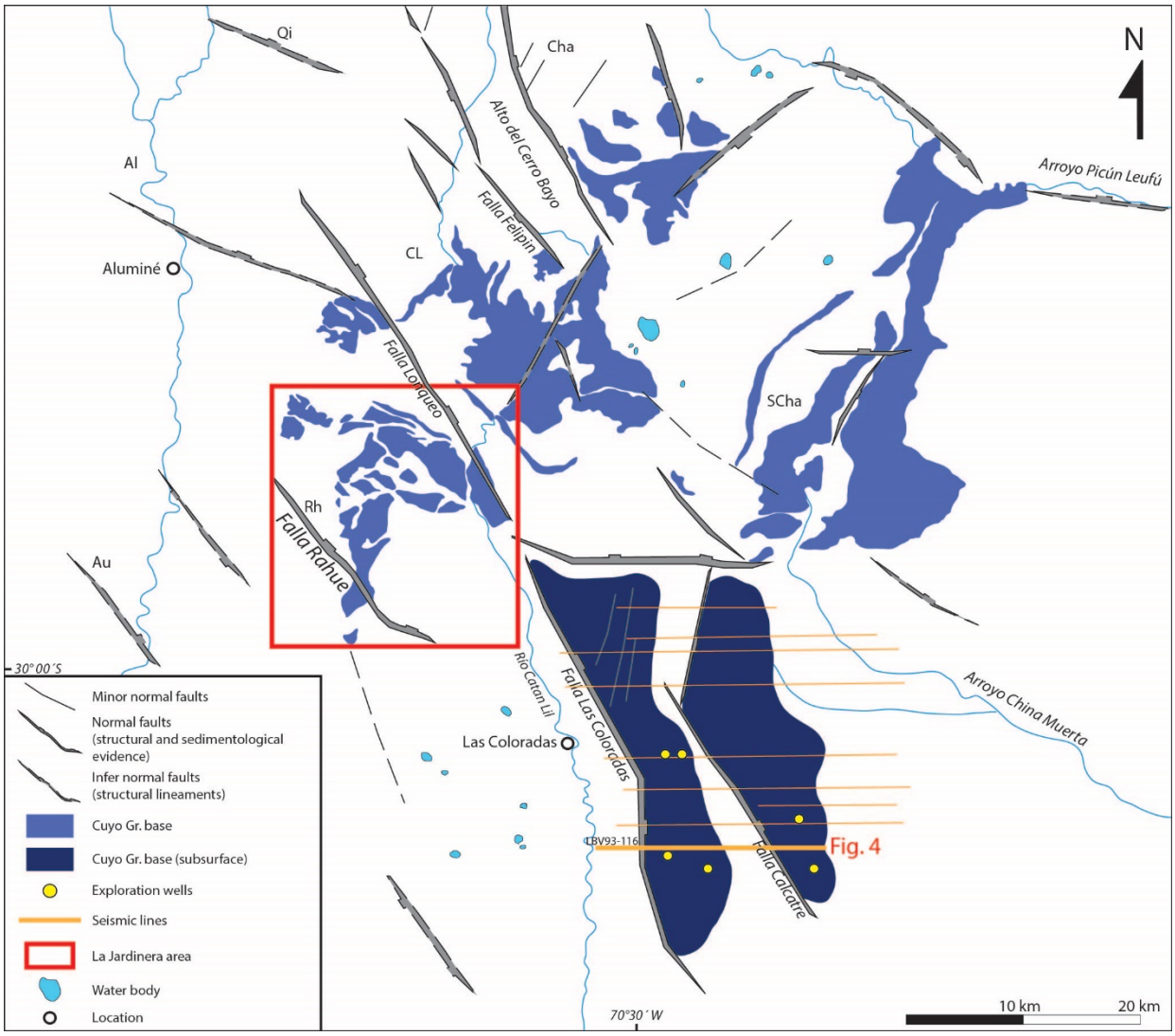

Figure 2. Distribution of hemigrabens and their associated faults and deposits of Cuyo Gr near the study area (modified from Morabito, 2010). The indicated seismic line is presented in Fig. 4.

During Early Jurassic times, extensional faulting was an important control on sedimentation on Neuquén Basin (Fig. 1 and 2), with thick accumulations of marine strata confined to depocenters (hemigrabens) bounded by horst blocks (Vergani *et al.*, 1995).

In La Jardinera and surrounding areas, a fault system with a northwest – southeast orientation was described by Morabito (2010; Fig. 2). These faults delimitate different depocenters in which the base of Los Molles Fm. is controlled by the geometry given by the hemigrabens, either in outcrop or in subsurface. According to Morabito (2010), the basal deposits Los Molles Fm. in La Jardinera area were deposited in a hemigraben controlled by Rahue Fault (Fig. 2 and 5). We can see on a seismic line proximal to La Jardinera (Fig. 4), how the base of Los Molles Fm. onlaps the small hemigraben geometry. The high amplitude reflectors might be indicative of sandy deposits that are onlapping the borders of the hemigraben.

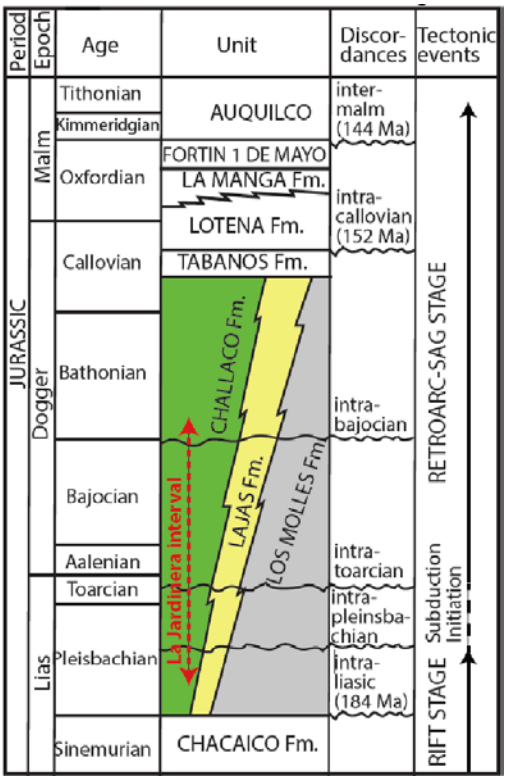

Figure 3. Stratigraphy and main tectonic events for the Jurassic of the Neuquén basin (Gulisano *et al.*, 1984; Vergani *et al.*, 1995; Paim *et al.*, 2008; Olariu *et al.*, 2019)

Relative changes of sea level during the development of the stratigraphy have been recorded and interpreted by Legarreta & Gulisano, (1989) and Legarreta & Uliana, (1996), who associated the entire Cuyo Gr to a stratigraphic sequence of second order (as defined Haq *et al.*, 1987). They interpreted a shoreline retrogradation associated with transgression during Pliensbachian – Toarcian followed by large-scale progradation (regression) during Aalenian –

Bathonian times and lastly a sea-level fall that ended with desiccation of the basin and deposition of evaporites in the Callovian.

Burgess *et al.* (2000) suggested that, during the Pliensbachian, the complex faulted topography was an important control on sediment routing in the southern areas of the basin. Their petrographic data indicates a dominant supply from the volcanic arc to the west, although paleocurrents from the same study show current-flow directions to the northwest, evidencing complex pathways through the fault system probably associated with relay ramps between distinct depocenters.

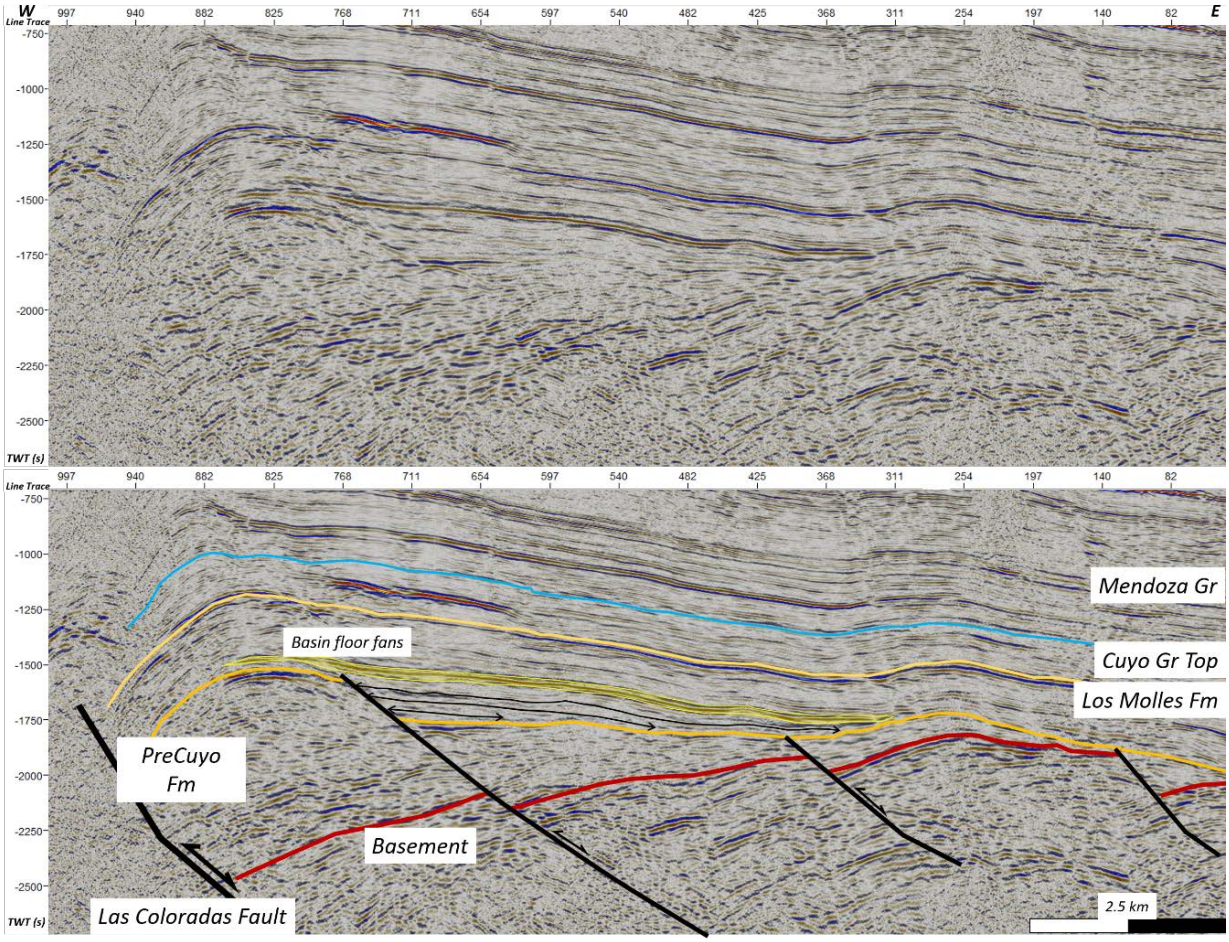

Figure 4. Seismic line-oriented W-E and structural interpretation. An inverted hemigraben is recognized, with one major fault to the west and smaller scale faults towards the east. Note that one of the faults is creating accommodation for the base of Los Molles Fm. (arrows). The high amplitude reflector on Los Molles Fm. colored in yellow is interpreted to be a sandy deposit probably associated with deep water fans. Note the terminations of the reflectors in Los Molles Fm. base towards relative highs. Courtesy of Pluspetrol S.A.

3. Data and Methodology

This study has made use of a high-resolution satellite image (0.5 m) with a Digital Elevation Model (1 m resolution) that was then interpreted to build a stratigraphic framework (Fig. 5). Part of this work was made by previous authors (Paim *et. al.* 2008; Tudor, 2014; Shin, 2015); the intention here is to enrich the interpretation and focus on the lowermost part of the stratigraphy. Time-lines and large-scale architectural elements were mapped to understand the continuity and correlation between the measured sedimentary logs.

Approximately 4,000 m of logs were measured in detail in 18 different locations distributed in the area to have a good understanding of the entire lower Fan in three dimensions. Of these 18 measured sections, 8 were measured by Shin (2015), who worked an interval of the same basin floor deposits in the area (Fig. 5A).

Description of the rocks focused on grain size, sedimentary structures, bed thickness and bed geometry. Grain size of each bed was measured thoroughly in order to establish within-bed trends and distributions as well as trends between successive beds. This was possible to do in outcrop due to the overall coarse-grained nature of the deposits (medium to very coarse-grained sandstones and conglomerates). Even though there was not a great variety of sedimentary structures present in the deposits, it was important to recognize them to help understand types of flow. Bed characteristics like thickness, geometry, degree of erosion and amalgamation are a key part of this study to better understand location within the depositional environment and architecture of the fan.

Over sixty paleocurrent measurements mostly from erosive features at the base of the beds (e.g. flutes, groove casts) were used to understand paleoflow variability (Fig 5B). Main direction of the flow is towards NE–NNE but there is also indication of northwesterly paleoflows, which suggest multiple sources, or tortuous pathways to the deep-water fans (Fig. 5).

In addition, photomosaics and large-scale drone photography were used to help correlation between logs and identification of large-scale channelized geometries vs poorly or non-channelized architecture.

All these sedimentological observations where used to characterize facies and facies associations.

In the La Jardinera basin-floor setting, four main depositional environments are interpreted, used and being guided by published works elsewhere that focused on facies and architectural

elements of the basin floor (Prélat *et al.*, 2009; Koo *et al.*, 2016). These four are *lobe axis*, *lobe off axis*, *lobe fringe* and *channels* (Fig. 6). In addition, a hierarchical scheme was adopted to partition the elements into different scales (Fig. 7). Consequently, 5 lobe complexes were identified based on thick (2.5 – 7 m) shale intervals occurring between these complexes; 3 to 6 lobes are interpreted in each of these lobe complexes; each of the lobes is formed by stacked event beds.

The measured outcrop logs were loaded in Petrel software as well logs. Thickness maps and Net to Gross maps for each lobe complex were created in Petrel software after correlation between all measured sections in order to provide a stronger framework of interpretation for the facies associations and better understand the evolution of the system.

Facies, grain size, bed thickness and net to gross ratios constituting lobes 3 and 4 of Lobe Complex 3 were plotted in frequency histograms to identify distribution patterns and therefore build a stronger interpretation of the units forming lobe complexes.

A qualitative determination of bed thickness and grain size trends within lobes was made in 3D in order to interpret types of stacking and the possibility of progradation within single lobes.

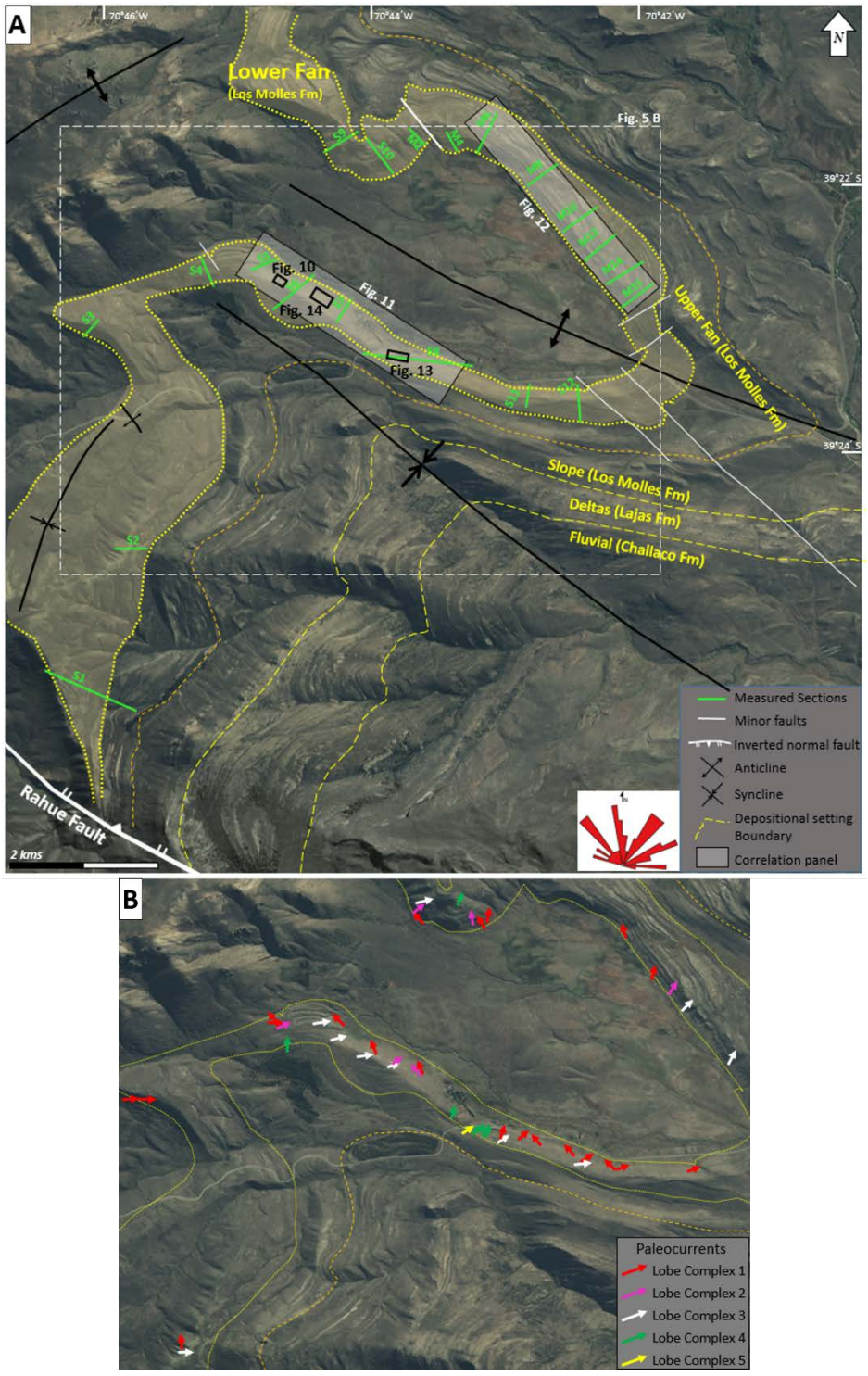

Figure 5. A- Satellite image of La Jardinera area with the acquired data and the regional geological interpretation. The present work is on Lower Fan at the base of the succession (interpretation modified from Paim *et al*., 2008). B- Zoomed in image of La Jardinera area with acquired paleocurrent data classified by the major hierarchy on the basin floor fan.

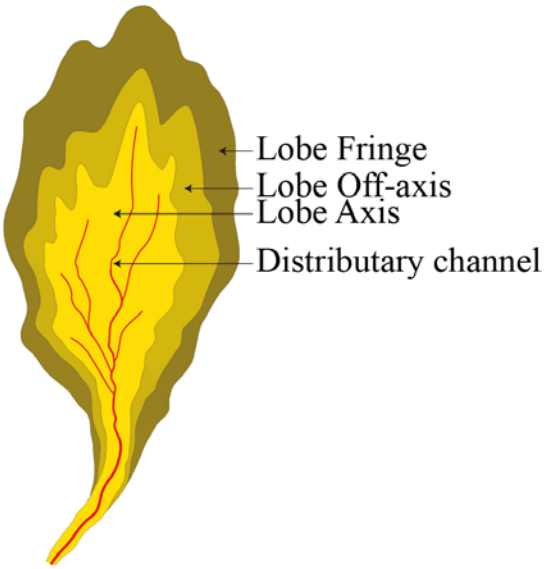

Figure 6. Schematic plan view of a lobe indicating the nomenclature used to describe different components and environments of lobe systems (modified from Prelat *et al.*, 2009).

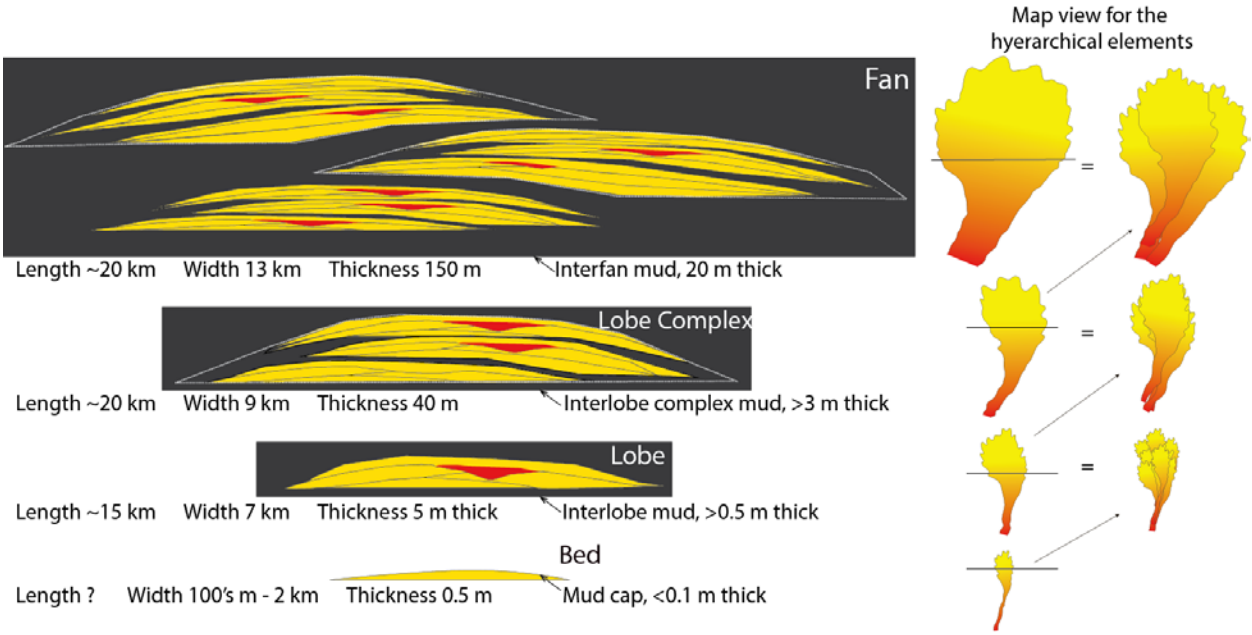

Figure 7. Hierarchical scheme adopted to interpret different scales of elements in the basin floor fan. Colors red to yellow are indicative of changes from channelized to unconfined elements (conglomerates to sandstone respectively)

4. Results

4.1. LITHOFACIES AND FACIES ASSOCIATION

Lithofacies are defined here as units with similar lithology (grain size, structures and fabric), bed contact, thickness and amount of mud; lithofacies' uniformity is important, representing similar conditions of sedimentation. We defined 10 facies (table 1 and Fig. 8): Mudstone, interbedded silty mudstone and sandstone, normal graded sandstone, structureless sandstone, planar laminated sandstone, ripple laminated sandstone, matrix-supported paraconglomerate, normal graded clast-supported orthoconglomerate and hybrid beds.

The stacking of different lithofacies and the analyses of their respective geometries portray relationships that lead to grouping into several facies' association (table 2 and Fig. 9) that in this deep-water marine setting represent; hemipelagic deposits (FA1), fringe/distal fringe lobe deposits (FA2), off-axis lobe deposits (FA3), on axis lobe deposits (FA4), channel to lobe transition deposits (FA5) and debris flows (FA6).

Deep-water sediment gravity flow deposits have been intensely studied in terms of processes and therefore, several classifications exist. One of the first classifications, from Middleton & Hampton (1973), classified flows in terms of sediment support mechanism, focusing on turbulence, upward water movement of fluidized flow, grain-to-grain dispersive stress as grain flow and matrix strength in debris flow. Some authors (e.g., Talling *et al.*, 2012 and Mulder & Alexander, 2001) summarized many processes described and interpreted in the literature while building their own scheme for sediment gravity flow deposits. They have generally emphasized the key variables as (1) the concentration of sediment in the flow (hyperconcentrated density flows, concentrated density flows and purely turbidity flows, or high-versus low-density turbidity currents with 10% concentration as the boundary condition) and (2) percentage of mud in the flow (cohesive and non-cohesive flows). During the last decade, there has been a switch of interest from triggering mechanisms for turbidites, such as the classic slope-collapse/slumping trigger or the river flooding and generation of hyperpycnal flow with plume collapse (e.g. Mulder *et al.*, 2003; Zavala *et al.*, 2011), to more recent focus on processes that happen during turbidite movement such as hybrid or transitional aspects of the flows (Haughton *et al.*, 2009; Sumner *et al.*, 2009; Baas *et al.*, 2011; Kane & Pontén, 2012). The latter was first described as slurry flows (Wood &

Smith, 1957; Hampton, 1972), with structures supporting evidence of flows going through a turbulent to a laminar transition.

Talling *et al.*, 2007, 2012 and Haughton *et al.*, (2003), among other authors, emphasized the transformation some flows can suffer in time in a downdip direction. These transformations can be from dense to dilute flows as they decelerate and take in water (e.g. as in the classic Bouma turbidite), or they can be changes in the opposite way, where increasing mud content can lead to increasing fluid viscosity, yield strength and pore pressure and leading to debris flows.

On this work, we will mostly use classifications of coarse grained turbidites from (Lowe, 1982) and fine-grained turbidites by Bouma, (1962). We will mention but not discuss in detail the deposits of hybrid flows (Haughton *et. al.* 2003) and hyperpycnal flows (Mulder *et. al.* 2003).

Table 1 and Fig. 8 summarizes the facies that will now be described.

4. 1. 1. Facies

Facies 1 (F1) Dark Mudstone

Facies 1 consists of beds or units of finely laminated dark shales and silt, rich in organic content (Villar *et al.*, 2005) and with very little bioturbation. Facies 1 intervals varies in thickness but can be from several meters to hundreds of meters thick, as the classic Los Molles Fm. in the area when no coarse-grained gravity flow deposits are present. Ammonites and bivalves, generally preserved in concretions, occur in Facies 1.

Interpretation. These shale intervals generally represent suspension settling of pelagic and hemipelagic mud. Geochemistry analysis of these shales had been carried by different authors (e.g., Cruz, 2002; Villar *et al.*, 2005), showing that TOC values can range from 2 – 3.5 % and oHI (original hydrogen index) values of 500 mgHc/grTOC.

Facies 2 (F2) Interbedded silty mudstone and sandstone

Facies 2 consists of dark laminated shale and siltstone intervals 1–20 cm thick that intercalate with very fine to occasionally coarse sandstones less than 1 cm to 10 cm thick (Fig. 8 A). Units of F2 total thickness can be up to 20 m. The sandstone beds are sharp, with main sheet-like geometry over outcrop distance (100's m to kms) although minor scouring and fill of some beds lead to a lens - like geometry. The sandstone beds are structureless or normally graded and sometimes have a capping ripple lamination on the top of the bed, as well as sparse rip-up

mudclasts inside the bed. The deposits of facies 2 commonly show soft sediment deformation that will be described subsequently. Most of the poorly exposed and covered areas on this region correspond to facies 1 and 2.

Interpretation. Facies 2 represents an alternation of muddy suspension settling and sandy event beds from dilute, low-density turbidity currents (Td and Te in the Bouma sequence). It is not the goal of this report to differentiate mud that settled out of turbulent suspension from hemipelagic and pelagic mud, but we recognize that both play a role. The erosive features at the base of some sandstone beds and the mudclasts are indicative of the turbulence of the flow that generated the deposits, both consistent with a low-density turbidite interpretation.

Facies 3A (F3A) Normal-graded sandstone

Facies 3 comprises sandstone beds of medium to very coarse grain size that grades normally to upper fine or medium grain size respectively (Fig. 8 D and E). Bed thickness varies from 10 to 70 cm (40 cm on average) in the case of medium grain size sandstones and from 40 to 150 cm (0.80 cm on average) for coarse and very coarse-grained sandstones. These deposits are generally poor to moderately sorted although sometimes they are well sorted. There are two types of normal grading recognized; one is the classic normal grading where mode or average grain size fines upwards; the other is a coarse-tail grading, where mainly coarse, very coarse and granules clasts diminish their content towards the top of the bed. The base of the beds is sharp, planar and non-erosive (few or nonexistent flutes) to slightly concave up and erosive. Beds with this type of erosive bases are laterally amalgamated and it is sometimes difficult to differentiate different events. The geometry of the sandstone units is generally tabular to undulating (high width/height ratio), although they present wedge shapes when are erosive and could form amalgamated meters thick sandstone bodies (Fig. 9 B). It is common to find loading at the interface of the beds. Rip-up mud-clasts are another common feature on these normal graded beds; they are found mostly at the top of the beds since they were more buoyant or hydrodynamically light and this helps to discern one event from an overlying amalgamating one. The mud-clasts vary in size from 2 cm to 10 cm (measuring b axes), are well rounded and are mostly oriented parallel to the bedding.

Another common feature that helps separate different event beds in amalgamated units are granules or pebbles concentrated at the base of each bed. Some centimeter scale inverse grading

of coarse material at the base (traction carpet) can also be found. Many times, but not always, this facies grades into facies 3C (laminated sandstone, Fig. 8 E).

Some of the thinner beds (10 to 20 cm) contain abundant plant phytodetritus at the top, closely related to facies F3C. The content and size of the detritus vary though it can be very high and as large as 5 mm.

Interpretation. This facies is interpreted as a deposit related mainly to low density turbidity currents, but sometimes the coarser basal part of the bed can reflect an early high-density flow. As the turbulent flow decelerates and loses energy, the sediment settles out of suspension (Talling *et al.*, 2012). The different grain sizes and therefore the density of the material, as well as the deceleration, is responsible for the grading, the heavier clasts being the first to deposit (Talling *et al.*, 2012). It is common to find coarse grains aligned throughout the bed, and especially near the base of the bed; this is interpreted to form as bedload movement while the settling of the finer material was still ongoing. The inverse grading at the base of some beds can be explained in terms of dispersive stress in traction carpets, where sediment concentration at the base of the flow is very high, and sediment support is dominated by grain collisions, though the bulk of the overlying flow is supported by turbulence (Lowe, 1982; Sohn, 1997). The mudclasts are evidence of turbulence and erosive capacity of the flow upstream. Since most of them are found at the top of the graded bed this could mean that they could be maintained in suspension by the turbulence of a flow. Beds with a high content of plant detritus is evidence of a direct source from rivers to the basin floor, making it likely that the turbidity current might have been triggered as a hyperpycnal flow.

Facies 3 B (F3B) Structureless sandstone

Facies 3B consists of upper fine to lower coarse-grained, structureless ungraded sandstone beds (the mode being medium; Fig. 8 B and C) of 10 to 60 cm thickness (40 cm in average) and occasionally up to 80 cm, although it is possible that thick beds represent locally amalgamated events. These sandstone beds can be well sorted or moderately sorted, with granules and very coarse clasts sparse throughout the bed. The base of the beds is sharp, sometimes showing evidence of erosion (flutes and groove) but with no deep scours. The bed geometry is locally tabular and it generally forms amalgamated packages, which makes it difficult to discern different events. Soft sediment deformation structures such as loading and flame structures are a common feature at the

interface of each bed (Fig. 8 B). Rip up clasts such as the one found on F3A are also present in this facies, but in less abundance. Some beds present moderate to high content of phytodetritus.

Interpretation. The structureless sandstone beds are attributed to very rapid fallout and accumulation of sediment, such that traction at the base of the bed is inhibited and sediment cannot be reworked (Middleton & Hampton, 1973; Lowe, 1982). The lack of lamination or evidence of basal traction, suggest deposits of the classic high-density turbidite with >10% sediment concentration in the flow. This rapid fallout traps high water content in the sediment and can cause liquefaction when another bed is swiftly deposited on top, which leads to fluid scape features and loading. The flute marks, though not as common as in F3A show evidence of localized erosion prior to deposition. Rip up mudclasts are a sign of the flow being turbulent and with erosive capacity upslope. The occurrence of phytodetritus is indicative of a direct linkage between the basin floor and the continental source (shelf-edge deltas).

The amalgamation of these deposits makes it difficult to discern different events when there are no changes in grain size from one flow to the next one.

Facies 3C (F3C) laminated sandstone

The laminated sandstone (Facies 3C) has two sub-facies separated (F3C-a and F3C-b) based on the laminae thickness and grainsize. Facies 3C-a consists of upper fine to medium sandstone with fine scale planar lamination (<5 mm; Fig. 9 E). The beds are generally thin (5 – 15 cm) and usually better sorted than other facies. Their base is non-erosive, sharp or transitional from facies F3A-B and they can be more discontinuous than the bed below. It is common that fine lamination associates with an alignment of small mud-clasts or phytodetritus on top of the graded sandstone. The lamination can be faint, making it sometimes difficult to recognize; waterscape features can disrupt it. Parting lineation can be sometimes present, which serves as paleoflow indicators.

There is another type of lamination that could be differentiated (F3C-b) since it has coarser grains, thicker laminas (>5 mm) and forms thicker beds (up to 40 cm). This laminated sandstone does not occur at the top of F3A-B. This may be the “stepped” lamination of Talling *et al.* (2012).

Interpretation. The planar lamination is associated in both cases with deceleration and rapid, but lamina by lamina fallout from an overlying low-density turbulent flow and the formation of a near-bed layer in which traction and granular interactions dominate and turbulence is damped.

The layers are driven by the overlying flow such that velocities are greatest in the upper part of the layer (Vrolijk & Southard, 1997; Sumner *et al.*, 2008 *apud* Talling *et al.*, 2012). In the case of 3C-b, where the laminae are thicker and coarser, the lamination is possibly related to higher concentrated flows (high-density turbidity currents) in which the settling is hindered and there is no normal grading.

Facies 3D (F3D) Ripple laminated sandstone

Facies 3D comprises upper fine to lower medium sandstone with ripple cross lamination (Fig. 8 A) and climbing ripple lamination (higher aggradation). The ripples present wavelengths of approximately 10 cm although some are smaller (2-3 cm) and occur in beds no thicker than 5 cm. They generally occur at the top of F3C or in F2 intervals. As well as with F3C, there are also coarser and thicker sandstone beds (upper medium and 10 cm thick) that exhibit ripple cross lamination. The base is non-erosive and the beds tend to be discontinuous. At locations where erosion is significant, bed amalgamation occur and facies 3D can be eroded by the next turbidite flow event.

Interpretation. Fine-grained, ripple cross lamination represents deposition from a dilute and fully turbulent suspension, with low rates of fallout (Southard, 1991; Baas, 1994 *apud* Talling *et al.*, 2012) in which the sediment is then transported by traction. In the case of the thicker and coarser grained ripples, they can be formed in areas where the flow expands and produces a hydraulic jump (Jobe *et al.*, 2012).

Facies 4 (F4) Matrix supported paraconglomerate

Facies 4 consists of very poorly sorted, matrix-supported granule to boulder conglomerate with a mud rich matrix (Fig. 8G and H). Some units consist of granules only, while others comprise the whole spectrum mentioned before. The bed exhibits no organization at any level; no grading or imbrication is seen. The clasts mainly consist of lithic fragments (mud-clasts, sandstones, volcanic and granites). The matrix, although mud rich, has sand grain size as well (from fine to very coarse). Beds range from 50 cm up to 5 m, have sharp non-erosive bases, sometimes undulating.

Facies 4 beds are usually present in the muddy intervals and are generally associated with deformed and contorted beds below and above. They are present in many measured sections and can be correlated for 100's of meters.

Interpretation. This facies is interpreted as a classic debris flow deposit. The mud provides cohesiveness and matrix strength and this is the main grain support mechanism as the current flows downdip. The debrite forms by abrupt *en masse* deposition (freezing of the flow) in which larger and smaller grains in the matrix tend not to segregate due to the strength of the matrix (Talling *et al.*, 2012). Due to the laminar behavior of the flow they tend to be non-erosive and do not incorporate material into the flow. Nonetheless, the strength of the mass flow (mainly due to its very high density and cohesiveness) can cause slumping and sliding of previously deposited unconsolidated material (Fig. 8G).

Facies 5 (F5) Normal graded Orthoconglomerate

Facies 5 consists of clast-supported to partially clast-supported conglomerate beds in a poorly sorted sandy matrix composed of medium to very coarse grain size clasts, grading upward into conglomeratic sandstone and coarse to medium sandstone at the top, where there is sometimes a faint lamination (Fig. 8 I and J). Beds range in thickness from 20 cm up to 1.5 m and are generally laterally continuous although they present great changes in thickness. The geometry is generally concave up in the thicker parts to tabular when thinning laterally. Most of the coarse-grained material is concentrated at the base of the thicker beds. The base is sharp, usually highly erosive (scours up to 2.5 m); flutes and groove marks are a common feature and serve as good paleoflow indicators. Facies 5 forms amalgamated bodies and it is sometimes difficult to discern different flow events. Sometimes beds can be separated when there is inverse grading at the base of beds prior to the normal grading.

Interpretation. Facies 5 represents deposits from a decelerating high-density turbidity current (coarse-grained turbidites, Lowe, 1982; Mutti, 1992). Due to the grain size, it is more likely that turbulence itself did not account for the main support mechanism, but that it was accompanied by grain to grain interactions and dispersive flow pressure. As grains start to settle at the base of the flow, inverse grading can occur in response to dispersive pressure, creating traction carpets. Although not entirely turbulent, these flows show evidence of being highly erosive and so are not associated with sandy debrites. Scours can sometimes have steep almost vertical sides; it is likely

that they are preserved due to very rapid deposition after erosion, and this means that they were probably filled by the same flow that caused the erosion. Although this facies represents a small percentage of the total deposits (approximately 10%), it is found on most sections and they can be correlated between different locations.

Facies 6 (F6) Hybrid beds

Facies 6 is composed of structureless, fine to lower coarse sandstone that abruptly grades into muddy sandstone with faint lamination and occasional fluid escape features (Fig. 8 F). The top of the bed shows alternating sand and mud layers, with a "sheared" appearance. Mudclasts and laminated phytodetritus situated at the top are another common feature. Bed thickness ranges from 20 to 40 cm; they are laterally continuous at outcrop scale with no significant change in thickness. The base of the bed is sharp and non-erosive.

Interpretation. Facies 6 deposits represent sediment gravity flows that had experienced changes in flow behavior while material was settling. The lower sandy part of the unit represents rapid dumping of suspended sand from the turbulent head of the flow, while the upper part settled mud and sand creating a mix that continues to move downdip with a more laminar component due to the cohesiveness of the material and lubrication from water-scape (Haughton *et al.*, 2009). This type of flow is usually recognized on distal parts of the system (Haughton *et al.*, 2003).

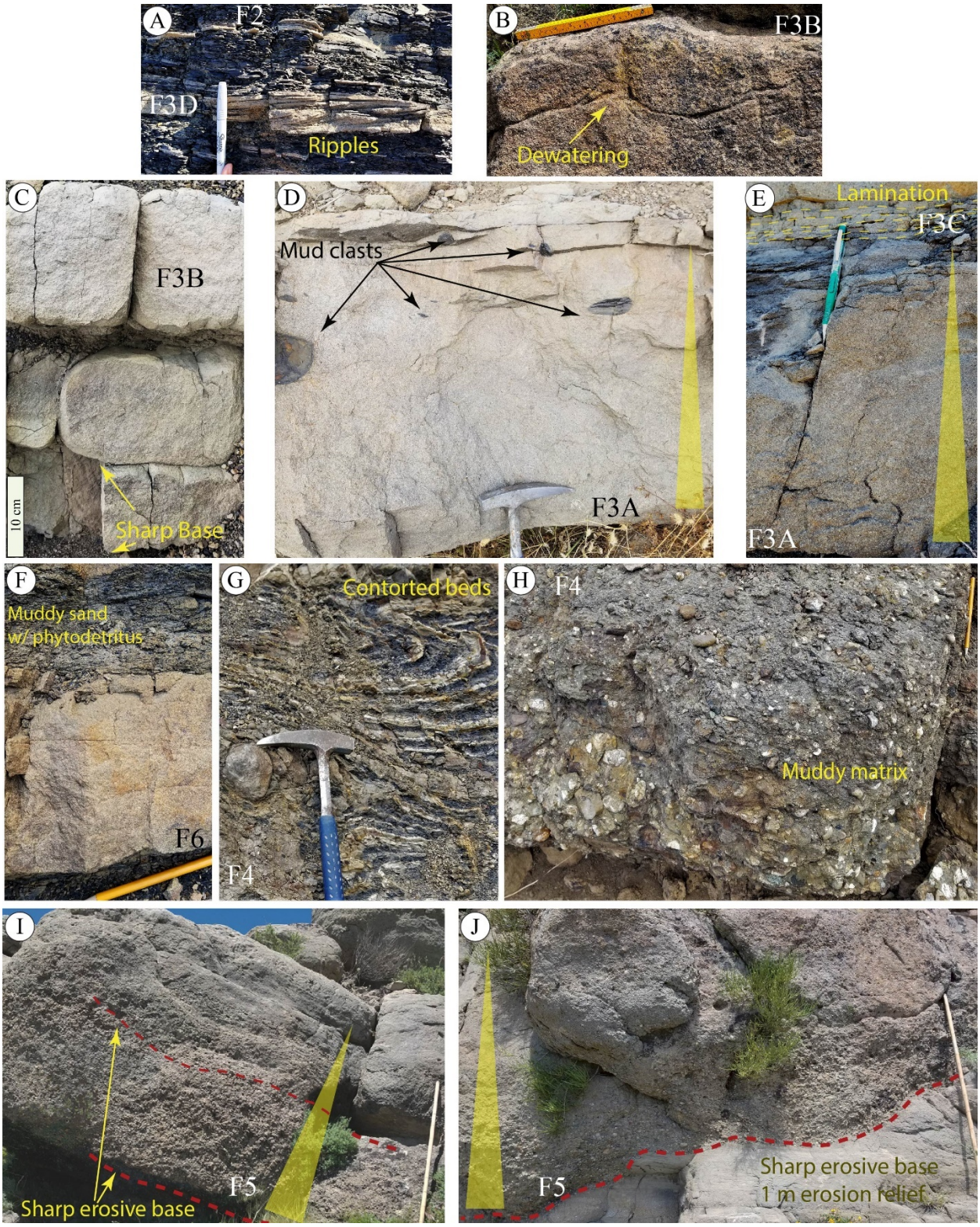
A
F2
F3D
Ripples
B
F3B
Dewatering
C
F3B
10 cm
Sharp Base
D
Mud clasts
F3A
E
Lamination
F3C
F3A
F
Muddy sand
w/ phytodetritus
F6
G
Contorted beds
F4
H
F4
Muddy matrix
I
F5
Sharp erosive base
J
F5
Sharp erosive base
1 m erosion relief

Figure 8.

Facies described and interpreted in the Lower Fan of Los Molles Fm. A- Interbedded silty mud – sandstone and ripple laminated sandstone (F2 and F3D respectively), B- Structureless sandstone bed with fluid scape features (F3B), C- Structureless sandstone beds (F3B), D- Normal graded sandstone with mud clasts at the top of the bed (F3A), E- Normal graded sandstone (F3A) to laminated sandstone (F3C), F- Structureless sandstone grading rapidly to muddy sandstone with high phytodetritus content (F6), G- Matrix supported paraconglomerate associated with contorted sandstone-mudstone beds (F4), H- Matrix supported paraconglomerate (F4), I- Normal graded orthoconglomerate with sharp erosive base (F5), J- Normal graded orthoconglomerate with sharp erosive base with 1 m erosion relief (F5).

Facies		Description	Interpretation
F1	Mudstone	Dark gray - black, organic rich, laminated mudstone.	Hemipelagic and pelagic deposits settling from suspension
F2	Interbedded silty mud - sandstone	Alternation of laminated silty mudstone with fine to coarse sandstone in 1 to 30 cms beds with sharp contacts, lenticular convex up or in sheets	Fine grained material settling from suspension associated with low density turbidity currents
F3A	Normal graded sandstone	Moderate to poorly sorted M - VC sandstone with sparse Gr that fine upwards to LM - UM sandstone. Higher concentration of Granules at base with coarse tail fining upwards. Ocacional inverse grading at the base (traction carpets). Rip up mud clasts generally concentrated at top. Ocacional groove casts at the base. Sharp to erosive bases. Bed thickness varies from 20 to 40 cms but bodies reach 1.5 mts when amalgamated	Settling of waning high to low density turbidity currents
F3B	Structureless sandstone	Good to poorly sorted F - C sandstone with sparse Granules, mudclasts and plant fragments. Sharp to erosive bases. Beds from 10 to 50 cms with wedge shape. Bodies reach 2 mt when amalgamated	Very rapid settling of High density turbidity currents or transitional flows
F3C a	Fine Laminated sandstone	Good to moderate sorted F - M sandstone with faint to clear lamination (<5 mm thick). Generally presented on top of normally graded sandstone. Beds have wedge to tabular shape, are 5 - 15 cm thick. Contact is transitional to sharp with facies below	Tractive deposits from wanning turbidity currents
b	Coarse Laminated sandstone	Moderate sorted M - C sandstone with faint to clear lamination (>5 mm thick). Beds have wedge to tabular shape, up to 40 cms thick and the contact is sharp	Stepped lamination. Tractive deposits from wanning turbidity currents (higher density than F3C-a)
F3D	Ripple laminated sandstone	F - C sandstone with ripples and ripple cross lamination. Generally on top of normally graded or laminated sandstone.Beds are 2 to 20 cms thick and laterally discontinuos following facies geometry below	Tractive deposits from waning low density turbidity currents
F4	Matrix supported paraconglomerate	Granule to boulder conglomerate with muddy matrix. Beds range from 30 cms to 5 mts, contacts are sharp and wavy. Soft sediment deformation associated	Plastic cohesive flow (Debris Flows)
F5	Normal graded Ortoconglomerate	Granule to pebbly conglomerate with sandy matrix which ranges from M to VC. Clast to matrix supported. Grades upwards loosing granules and pebbles. Beds range from 20 to 80 cms and are generally continuous with changes in thickness exhibiting planar to concave up geometries. Base of the bed generally erosive	Settling of waning high density turbidity flows and tractive deposits
F6	Hybrid beds	Massive F - LC sandstone grading rapidly into muddy sandstone with fainted lamination and ocacional fluid scape features Beds usually 20 - 40 cms, continuous with sharp base	Hybrid flows that exhibit a transition between turbulent to laminar regime

Table 1. Table showing 9 different facies described and interpreted in the Lower Fan of Los Molles Fm.

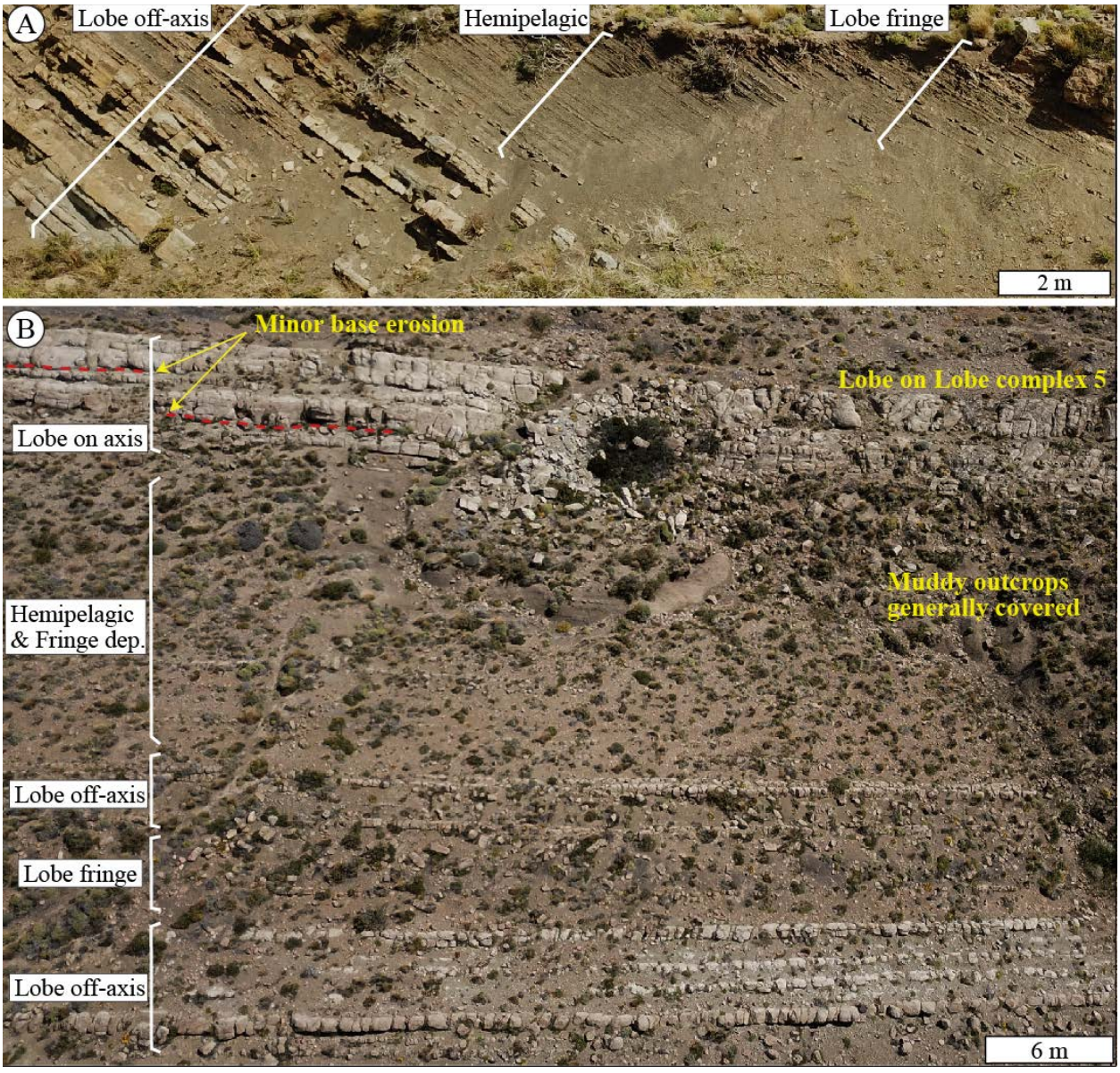

Figure 9. Facies Association examples from the Lower Fan in Los Molles Fm. A- Lobe off-axis deposits (FA3), Hemipelagic / pelagic deposits (FA1) and Lobe fringe deposits (FA2). B- At the bottom, alternation of lobe off-axis deposits (FA3) and lobe fringe deposits (FA2); at the top, lobe axis deposits (FA4). C- Lobe on axis deposits (FA4) partially eroded at the top by a distributary channel (FA5). D- Debris flows associated with contorted beds creating mass transport deposits (FA6). Continue next page.

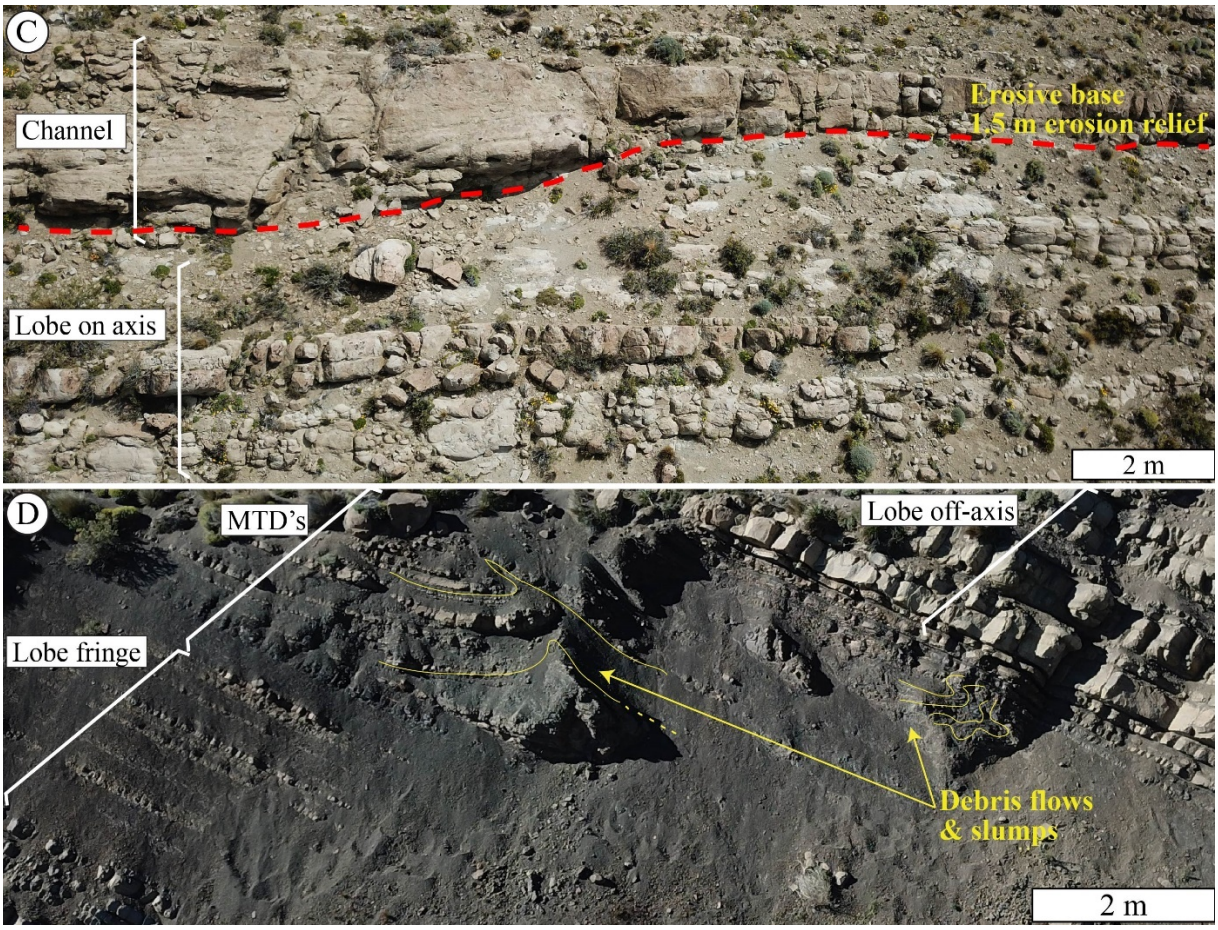

Figure 9 continued.

4. 1. 2. Facies associations

The described lithofacies are grouped into 6 facies associations that characterize a particular depositional environment on the basin floor fan (Table 2, Fig. 9). Each of these facies' associations will then be grouped in larger architectural elements following a hierarchal scheme.

FA1 Hemipelagic/Pelagic deposits

FA1 is represented only by F1. Facies 1 consists of finely laminated dark shales rich in organic content and very little bioturbation. They compose the slope and basin floor background for Los Molles Fm. in the area when no coarse-grained gravity flow deposits are present (Fig. 9A).

Interpretation. These thick shale intervals represent settling out of suspension of pelagic and hemipelagic deposits on distal basin floor areas and in areas of the slope where no coarse material is carried into the deep marine environment. They represent periods of quiescence or fan

abandonment in the deep-water system, where sea level was high and/or sediment input locally low.

FA2 Lobe fringe and distal fringe

FA2 facies assemblage consists of F1 (dark shales) and F2 (interbedded mud/silt and sandstone) with infrequent F3A (normal graded sandstone) and F6 (debris flows; Fig 9 A, B and D). Thickness of the association varies from 0.5 m to 10 m and it presents a sheet geometry. Intercalation of muddy and sandy packages appears to be random; nevertheless, there are intervals in which the amount of mud decreases towards the top, giving way to thicker sandstone beds.

Interpretation. This facies association represents the lateral and distal fringes of fan lobes. The sheet geometry of the beds, the amount of mud and the type of sandy facies that are found on this environment point to a dominance of unconfined dilute turbidity currents with occasional hybrid flows and debris flows that are being deposited on a distal position of the fan where there is also hemipelagic and pelagic material settling, contributing to the overall fine-grained appearance of the interval.

FA3 Lobe off-axis

A stacking of F3 (A, B, C, D) and F2 builds this facies association, not necessarily in that order (Fig. 9 A, B and D). They present an overall tabular arrangement and a lower N/G ratio (50 to 60%) compared to FA4 and FA5. The most common facies are F3A (normally graded sandstone) and F2 (interbedded silt/mud and sandstone). The off-axis intervals are 1.5 to 5 m thick with no clear vertical arrangement of the beds and facies.

The individual sandstone beds (F3 A-C) cannot be traced for long distances (10's to 100's m) and they usually pinch out laterally into previous deposits displaying a wedge geometry. Nonetheless, since there is more mud in these intervals it is easier to differentiate different flow events.

Interpretation. The intercalation of mud between the sandy deposits, the low N/G ratio and the overall tabular geometry of the deposits are good evidence of an unconfined system lateral to the main axes of the lobe where distributary channels feed the system. The amount of mud increases and the grain size and thickness diminish, relative to the main axis of the lobe, showing a more distal environment with fewer events reaching the area.

Individual beds are mostly interpreted as low-density turbidity currents. It is common to find normal graded sandstone capped by plane laminated sandstone and mud on top, showing a classic deposit formed by settling of material from a turbulent flow (Fig. 8 E). The wedge geometry and pinching out of the beds indicate local compensational stacking. When a lobe cannot continue to aggrade it shifts laterally towards a lower area as an autocyclic response (Hiscott, 1981).

FA4 Lobe on axis

This facies association consists of the assemblage of F3 A, B, and C with minor F2 (Fig. 9 B and C). These intervals show an undulating geometry with no large concave-up features. However, there is common evidence of minor erosion and scours at the base of some of the beds. Net to gross ratio is generally high, with values of 80 to 100%. Different event beds are stacked together forming highly amalgamated features; packages are 3 – 12 m thick. Three trends are recognized on this sub-environment; coarsening upward, thinning upward and amalgamation with no change in grainsize. This facies association correlates laterally to the previous one (FA3) and both represent most of the rock record analyzed on this work.

Interpretation. This association of facies is interpreted as unconfined, on-axis deposits of a lobe. The key to identifying these units resides in the stacking of the sandy beds, with amalgamated bodies, and the lack of large-scale erosive features. In areas proximal to the lobe axis, bed thickness as well as grain size increases due to the proximity of the feeding systems (distributary channels). The predominance of F3B (structureless sandstone) and F3A (normal graded sandstone) is also indicative of proximal or axial portions of a submarine lobe (see also Prélat *et al.*, 2009). The facies analysis suggests a predominance of high-density turbidity currents with minor participation of more dilute turbidity currents. Different stacking patterns suggest lobe shifting along the axis; mostly laterally with minor forward stacking components, as it will be discussed below.

FA5 Distributary channels & channel to lobe transition

The FA5 association of facies consists of F5, F3A, and F3B with occasional F3C (Fig. 9 C). The geometry of the beds is predominantly lenticular (concave up) to undulating, with erosive bases that can scour down as much as 2.5 m. These erosive surfaces amalgamate laterally into compound surfaces (Fig. 10 and 11) and can be traced for 10´s to 100´s of meters. Net-to-gross

ratio is high, with essentially no shale between beds, giving a highly amalgamated bed-set. The association shows a fining upwards trend consisting mostly of F5 (normal graded conglomerate) sitting on top of an erosive surface, with F3A and F3B on top, although not always present. It is composed of 2 – 5 beds and the maximum thickness (measured at the major scours) varies from 1 to 3 m for each channelized element. The lateral extension of this facies association varies from 10´s to 100´s m and it is closely associated with FA4 (Fig. 10).

Interpretation. This facies association is interpreted as distributary channels at a channel to lobe transition. The specific characteristics that support this interpretation are the scours and the conglomeratic units sitting on top, evidencing an important break in grain size. They are interpreted as channel to lobe transition due to the lateral extent that some of these amalgamated units have and their close relationship with unconfined deposits sitting on top (more details on discussion). Some of the smaller channels can be distributary, feeding lobes downstream towards the east. The channels might occur abruptly or transitioning from on-axis unconfined deposits (coarsening and thickening upward trends). Then, they grade upward to lobe deposits, showing an overall fining upward trend. This represents a very rapid event where the channel develops quickly, then the system backsteps or shifts and on-axis lobes deposit on top.

FA6 Debris flows and Mass transport deposits (MTDs)

FA6 is characterized by deformed masses of FA2 sandstone and mudstone, showing evidence of soft sediment deformation (usually contorted beds, Fig 9 D). They are always associated with F5 (debris flows) in fine-grained intervals. These MTDs are small considering the thickness these units can have on the sedimentary record; their thickness varies from 50 cm to 5 m. In some cases they create minor positive relief (1 m) against which the sandstone beds onlap.

Interpretation. The MTDs reported in this work are interpreted as a response of debris flows disrupting the underlying bed when decelerating and a decrease in hydroplaning (Mohrig *et al.*, 1998). As the debris flows decelerates, it excavates into the underlying unlithified deposits and drags them forward, producing slumped features. Since these cohesive debris flows associated with slumps occur in the finer grained intervals where there has been a smaller flux of sediment into the basin, they are interpreted as resultant from instability on the slope during late transgressions and early regressions (Cronin *et al.*, 1998)

Facies Association	Main Facies assemblage	Depositional environment
FA1	F1	Hemipelagic / pelagic deposits
FA2	F1+F2 (F3D)	Fringe lobe deposits
FA3	F3A + F3C + F2 (F3B + F3D)	Off axis lobe deposits
FA4	F3A + F3B + F3C	On axis lobe deposits
FA5	F5 + F3A + F3C	Channel to lobe transition - distributary channels
FA6	F4	Debris flows / MTDs

Table 2. Table showing main interpreted facies association with their respective facies' assemblage. Between brackets are secondary facies.

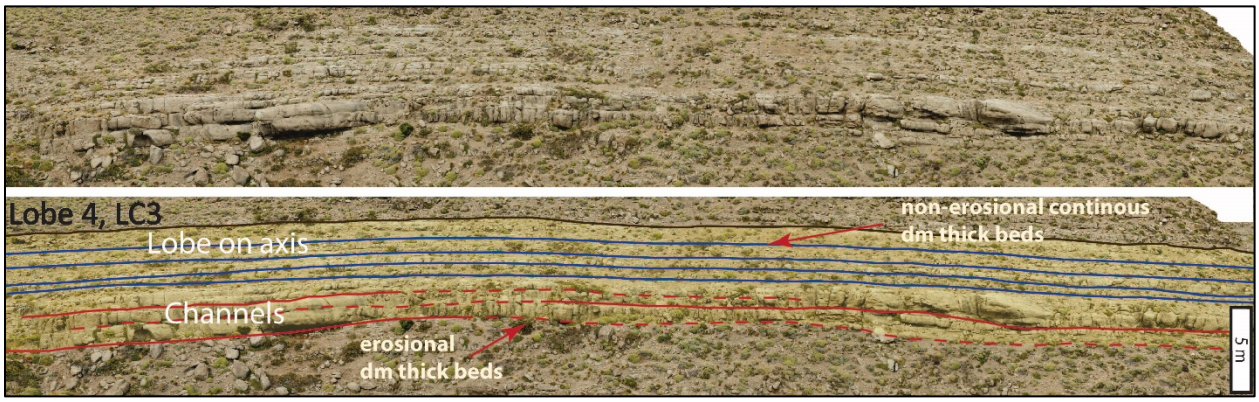

Figure 10. Photomosaic and its interpretation (top and bottom). Red lines represent the base of amalgamated distributary channels (FA5). Blue lines on top represent the base of unconfined on axis lobe beds (FA4). This image shows a good example of the different architectural elements found on a lobe. See Fig. 5A for location

4. 2. FAN HIERARCHY & ARCHITECTURE

Having interpreted facies and facies associations, we built a hierarchical framework to better understand how the system evolved from single flow events (beds) to larger assemblages (fans). To accomplish this task, we correlated all measured logs shown in figure 5 and used architectural features (Fig. 6) and a hierarchical scheme (Fig. 7) based on Prélat *et al.*, (2009); Prélat & Hodgson, (2013) and Koo *et al.*, (2016). This division begins with identification and correlation of significant fine–grained units between sandstone bodies. Due to lateral variation, it is not always an easy task to accomplish a proper hierarchical division of the different components in the fan; e.g. thin intervals of fine–grained units can laterally thicken; and what might have been interpreted as an interlobe deposit might actually be an interlobe complex.

Table 3 summarizes the hierarchy and architecture of the Fan. Figures 11 and 12 show 2 correlation panels with a transverse – oblique view of the interpreted fan. After a detailed correlation in 3 dimensions, we believe that panel 1 (Fig. 11) most clearly shows the adopted hierarchical scheme.

The minor unit identified in this hierarchical scheme is the individual bed that responds to a single flow event. These events stack together to form lobe elements, the different architectural parts of any lobe. These elements can either be a series of confined beds such as described in FA5 (small channels) or unconfined beds as in FA3 & 4 (on axis or off axis, depending on the location). The assemblage of stacked beds in different element architectures forms each lobe (Fig. 10). It is worth mentioning that the term lobe element as it is being used in this work differs from the concept portrayed in Prelat *et. al.* (2009), as we only use it to describe the architecture of the stacked beds and not as a hierarchical division of the lobe.

Seventeen lobes, each 5 – 10 m thick (6 m thick in average, measured on axis), were identified using facies association and shale intervals. Fine-grained units described as inter-lobe deposits range from 50 cm to 8 m and are represented by FA1 and FA2. There are parts of the fan succession where lobes are amalgamated, especially when small channels erode part of the succession, and it is more difficult to distinguish individual lobes. Lobes are therefore easier to recognize off-axis (e.g. Lobe complex 3, section 8, Fig. 11), where mud deposits are thicker; or on axis when not many erosive features and amalgamation occurs (e.g. section 8, of lobe complex 4; Fig. 11 and 13).

	Lobe Complex 1	Iterlobe complex	Lobe Complex 2	Iterlobe complex	Lobe Complex 3	Iterlobe complex	Lobe Complex 4
Outcrop perspective	Medial to distal		Medial		Proximal to medial		Medial to distal
Thickness (max)	45 m	6 m	20 m	5 m	40 m	8 m	59 m
Inferred width	-		7.5 km		10 km		8 km
Lobes depositional Architecture	Aggradational and Progradational to retrogradational pattern. Minor amalgamation		Agradational to progradational stacked lobes with lateral migration and minor amalgamation		Agradational to progradational stacked lobes with minor lateral migration and high amalgamation		Agradational stacked lobes with no amalgamation
Number of Lobes	2 - 3		3		6		6
Type of lobe element	Unconfinned and few channels		Unconfinned and few channels		Unconfinned and higher number of channels		Unconfinned (only one channel in section 2)
	320° - 350° & 65°		320° - 350° & 65°		75° - 90°		30° - 45°
Paleoflow directions	North - Northwest and East -Northeast		Northeast		East		Northeast

Table 3. Table summarizing the large-scale hierarchy of the Lower Fan and its main characteristics.

Lobes were grouped together into 5 lobe complexes (Fig. 11, 12 and 14). Thicker mud units were used to differentiate this higher-order assemblage. The thickness of the interlobe complexes varies from 3 to 15 m, depending on the position within the fan.

Although we recognize the importance of individual beds in the evolution of the lobes and ultimately to the fan, this work focuses on the large-scale assemblage and patterns at a lobe and lobe-complex scale.

Nevertheless, we will briefly describe the types of vertical trends recognized within the interpreted lobes in terms of their grain size and bed thickness and then further discuss their significance in the next section. Figure 15 shows examples of the different types of stacking patterns observed in panel 1 (Fig. 11) and 2 (Fig. 12). Case A; there is no apparent increase or decrease in grain size and bed thickness or it is very subtle, and so it is considered constant (example from section 6, lobe 3 in lobe complex 2). Case B; a coarsening and thickening-up trend followed by finning and thinning up trend (example from section 6, Lobe 3 in lobe complex 2). Case C; there is an abrupt change in grain size from shale to very coarse sand and conglomerate deposits which then gradually decreases in grain size and bed thickness (example from section 8, lobe 1 in lobe complex 5). Case D; an increase in grain size and bed thickness to a point where broad erosive surfaces are observed; follows a gradual decrease to finer and thinner beds topped by mud.

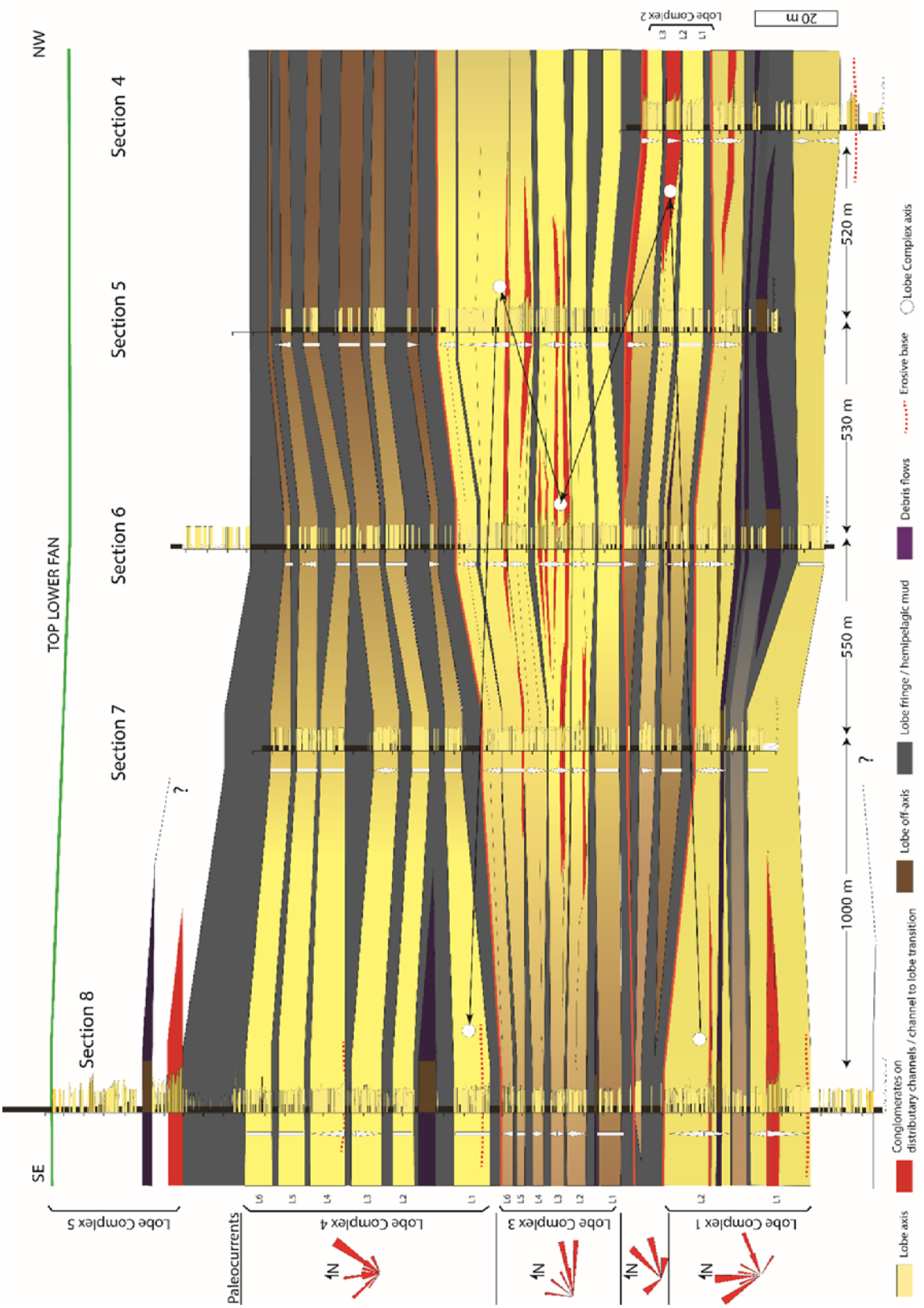
NW
SE
TOP LOWER FAN
Section 8
Section 7
Section 6
Section 5
Section 4
20 m
1000 m
550 m
530 m
520 m
Lobe Complex 5
Lobe Complex 4
Lobe Complex 3
Lobe Complex 2
Lobe Complex 1
Paleocurrents
Lobe axis
Conglomerates on distributary channels / channel to lobe transition
Lobe off-axis
Lobe fringe / hemipelagic mud
Debris flows
Erosive base
Lobe Complex axis

Figure 11.

Correlation panel 1 oriented SE to NW showing the major architectural elements and interpreted hierarchy of the Lower Fan (bounded by green lines) along an oblique / axial view. Lobe complex 5 is not interpreted due to lack of exposures in the rest of the panel. Grain size and bed thickness trends are indicated on the left side of the sections. Main paleocurrents are indicated to the left.

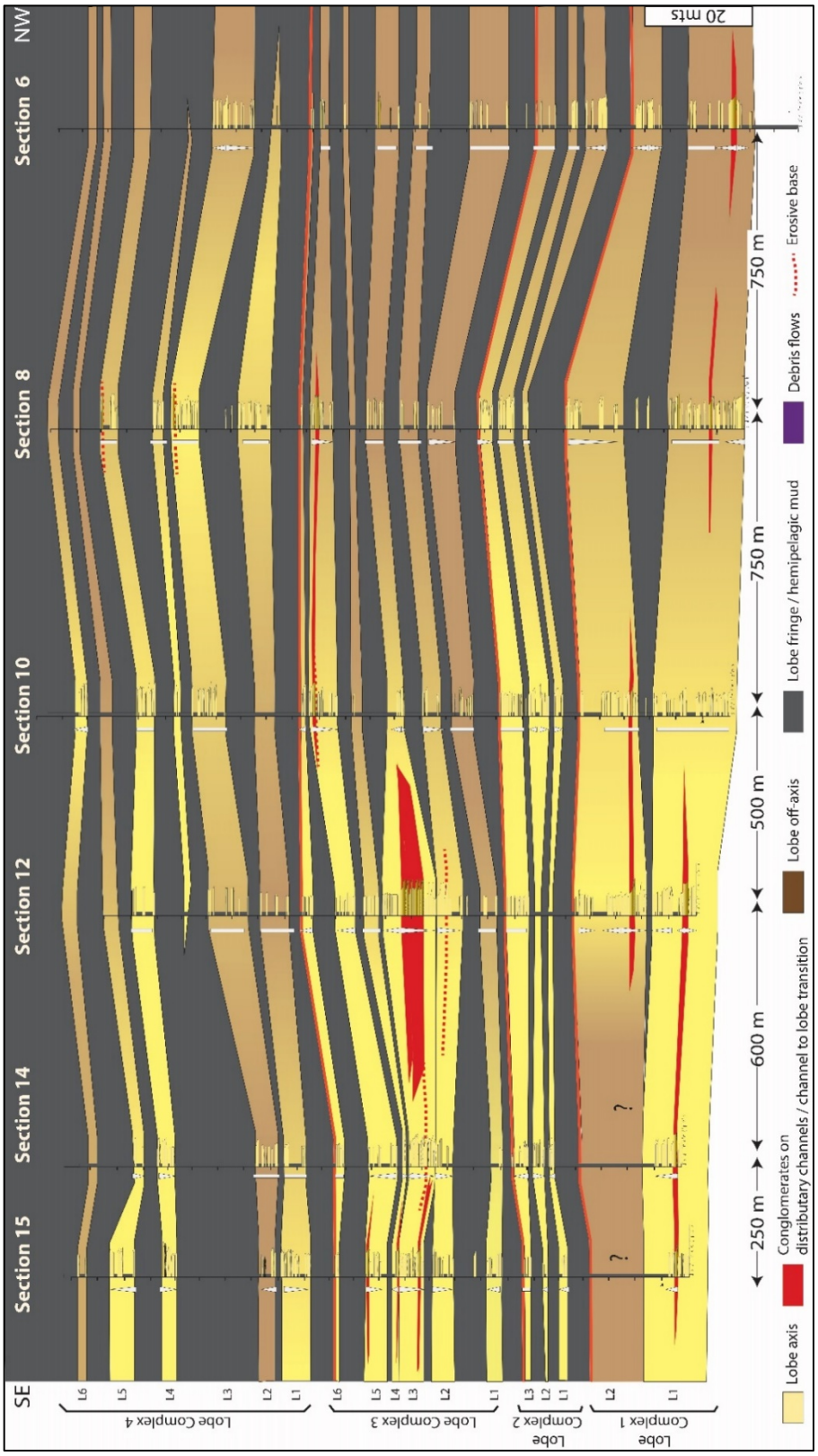
SE
Section 15
Section 14
Section 12
Section 10
Section 8
Section 6
NW
20 mts
Lobe Complex 4
Lobe Complex 3
Lobe Complex 2
Lobe Complex 1
L6
L5
L4
L3
L2
L1
250 m
600 m
500 m
750 m
750 m
Lobe axis
Conglomerates on distributary channels / channel to lobe transition
Lobe off-axis
Lobe fringe / hemipelagic mud
Debris flows
Erosive base

Figure 12.

Correlation panel 2 oriented Se to NW showing the major architectural elements and interpreted hierarchy of the Lower Fan downdip from panel 1 (Fig.12) along an oblique / axial view. Grain size and bed thickness trends are indicated on the left side of the sections.

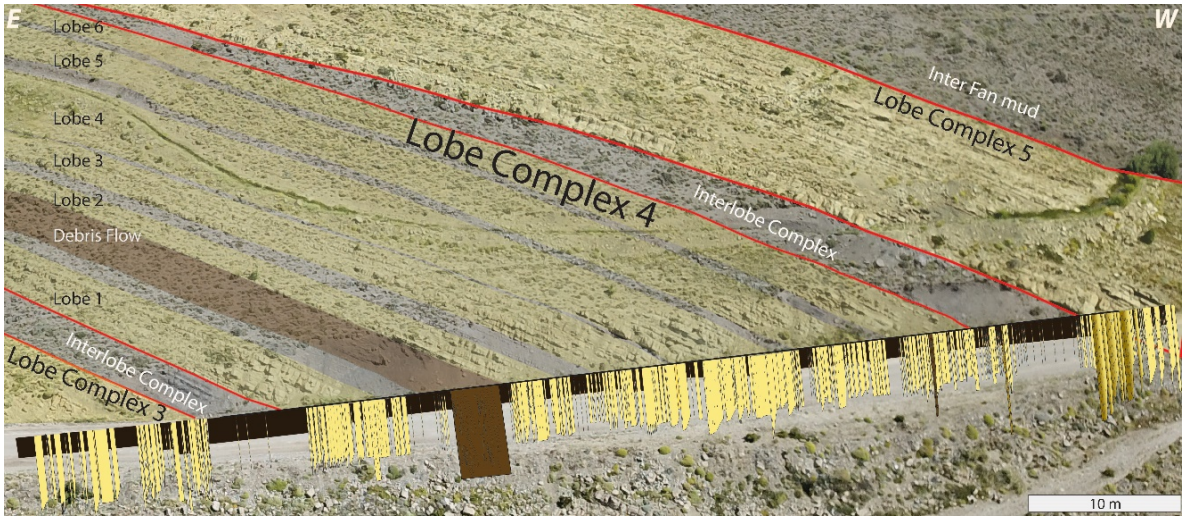

Figure 13. Aerial image showing hierarchical divisions on basin-floor deposits at lobe – lobe complex scale. This example is from Lobe complex 4, which shows 6 identifiable lobes separated by thin fine-grained intervals. See figure 5 for location.

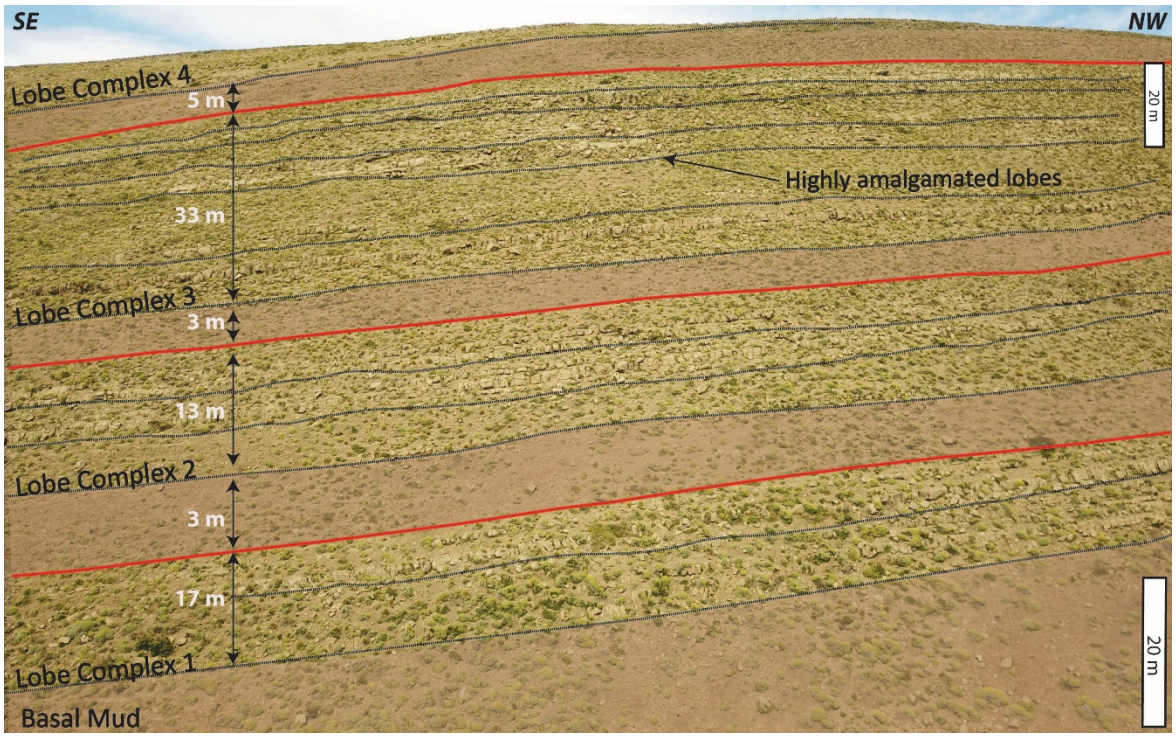

Figure 14. Aerial image showing hierarchical divisions within a basin floor succession at a lobe complex scale. The lower fan is composed by 5 lobe complexes, 3 of which can be seen clearly on this image; only the base of lobe complex 4 is seen here. Fine-grained intervals separate each lobe complex. On dash lines the base of the lobes. See figure 5 for location

4. 2. 1. Lobe complex characterization

Using previous described methods, 5 lobe complexes were interpreted within the basin floor fan studied in the area. A description for the first four lobe complex is presented, since the fifth is only well exposed in one section and was not correlated laterally throughout the area. We will repeatedly refer to panel 1 (Fig. 11) for guidance since it is where the basin floor fan is better exposed and it is here the hierarchical scheme was developed and then interpolated to the rest of the area. In order to provide a better framework of interpretation, thickness and net-to-gross maps were created in Petrel using as input all the measured sections and thickness trends observed from satellite images (Fig. 16). We will also briefly describe the stacking patterns recognized within the lobes that form the complexes (Fig. 15) which will be further discussed in the next section.

Lobe complex 1 (LC1)

The measured paleocurrents indicate 2 different directions of transport, one from the southeast towards the northwest, and another from the west-southwest to the east-northeast (Fig. 5 B). LC1 is considered the first episode of gravity flow sedimentation on the basin floor, situated on top of a thick succession of basin floor shales (200 to 300 m of FA1). This lobe complex is composed of 2 lobes with a possible third lobe poorly exposed at the base of the succession. Unlike lobes identified higher on the fan, these do not always show a clear subdivision, making it difficult to pick a clear boundary between each lobe.

The first lobe is composed mainly of laterally and aggradationally stacked unconfined elements (such as in Fig. 9 B and 10), with only a few channelized features to the southeast that represent the most proximal setting. A muddy interval with abundant debris flows follows, mainly occurring towards the northwestern site on panel 1 (Fig. 11). Next, a second lobe is identified, composed mostly of unconfined elements, although small scale channels are recognized to the southeast and northwest (Fig. 11).

The vertical pattern of sedimentation of the lobes varies laterally; there is a coarsening and thickening-up trend on section 8 (Fig. 11) whereas on panel 2 (Fig. 12) the pattern of sedimentation described above is not well observed; finer grained interval between sandy beds are more common and the stacking of individual beds seems more random with no clear trends.

Because the base of LC1 does not outcrop in the entire area, a thickness map of LC1 is not available; however, it is possible to build a NG map using only the LC1 thickness that is visible

on outcrop (Fig. 16). An irregular distribution of the sediment is visible; the southern part of the map shows a southeast-northwest distribution and the northernmost area a west-east distribution. Areas of low NG are located between these trends.

Lobe complex 2 (LC2)

Paleocurrents indicate a dominant direction of sediment transport towards the northeast (Fig. 5B). LC2 is composed of 3 lobes and it is separated from LC1 by a fine-grained interval (FA1 & 2) of 1 m to 5 m depending on the location. These lobes are laterally correlated to fine-grained material to the southeast on top of LC1 (section 8, Fig. 11).

The first lobe, although not obvious in outcrop due to its lateral extent, exhibits onlap to the southeast onto previous deposits of LC1. It is composed only by unconfined, poorly amalgamated bed-sets. The second and third lobe exhibit unconfined poorly amalgamated to amalgamated bed-sets with small distributary channels to the northwest (Fig. 11).

The vertical arrangement of the beds in terms of bed thickness and grain size do not follow a homogenous trend in the area. Some of the lobes show a coarsening and thickening-up pattern on specific sections (e.g. lobe 3 in section 5, Fig. 11) that it is not shared on other locations (e.g. section 14, Fig. 12).

The NG and total thickness maps of LC2 (Fig. 15) share a similar southwest-northeast trending distribution, with higher values at the northwest. The highest values coincide with the presence of the sediment entry points (channels), located near section 4.

Lobe complex 3 (LC3)

Paleocurrent measurements on LC3 indicate a dominant direction of sediment transport towards the east – northeast (Fig. 5B). LC3 is separated from LC2 by a fine-grained interval (FA1 & 2) of 1 to 5 m thick varying with the location. It is composed of 6 lobes that can be well defined off-axis at a SE location on panels 1 and 2 (e.g. section 8, Fig 11 and section 15, Fig.12).

Lobes in LC3 are mostly represented by FA4 and FA5 on panel 1 (Fig. 11), with minor deposits associated with FA3 towards the southeast. Lobes 1 and 6 are entirely composed by unconfined poorly amalgamated to amalgamated bed-sets. Lobes 2 to 5 are formed by amalgamated unconfined bed-sets and channelized elements to a minor extent. Lobe 3, in particular, presents the highest proportion of channelized features on the entire lower fan (between

sections 5 and 7 on panel 1, (Fig. 11). Lobes 2 to 5 on LC3 can be identified on panel 2 (Fig. 12) with similar characteristics in terms of facies association to those seen in panel 1, presenting FA4 and FA5 on sections 15, 14 and 12. The proportion of channels on LC3 diminishes in panel 2; the only ones that can be traced to the other side of the anticline correspond to lobe 3. Towards the northwest, sub-environments change from FA 4 & 5 to FA 2 & 3, moving away from the axis.

In terms of the vertical arrangement of the beds, lobes 1, 4, 5 and 6 show diverse patterns throughout the area, with no clear recognizable arrangement (Fig. 11 and 12). Lobes 2 and 3 on the other hand, are characterized by coarsening and thickening up and then fining and thinning-up trends in almost all measured sections (Fig. 11 and 12).

The NG and total thickness maps of LC3 (Fig. 16) share a similar southwest-northeast distribution; nevertheless, the highest thickness values are located slightly north to the highest NG values. The distribution of the deposits to the northeast is irregular, with finger-like geometries oriented towards the east-northeast and north (Fig. 16).

Lobe complex 4 (LC4)

Paleocurrent measurements on LC4 indicate a dominant direction of sediment transport towards the northeast. LC4 is separated from LC3 by a fine-grained interval (FA1 & 2) of 2 - 8 m depending on the location. It is composed of 6 lobes easily identifiable on panel 1 (Fig. 11 and 13), each one separated by <1 m to 5 m of FA2.

Lobes are composed almost entirely of unconfined elements, with the exception of one channel recognized on lobe 6, measured in section 2 (Fig. 5 A). On panel 1 (Fig. 11), facies associations vary laterally from FA4 on sections 7 and 8 to FA3 on a northwestern direction (sections 5 and 6). From southeast to northwest the level of amalgamation of the bed-sets in each of the lobes diminishes, as finer material increases between beds. Downdip, panel 2 (Fig. 12) shows a decrease in amalgamation of the bed-sets and an increase of fine-grained material represented by FA1 and 2.

The vertical arrangement of the beds on each lobe do now follow a uniform pattern in the area. While some lobes show a coarsening and thickening-up trend (e.g. lobe 3 on section 8, Fig. 11), laterally they present a thickening and coarsening-up trend followed by thinning and finning-up trend (section 7, Fig. 12).

The NG and total thickness maps of LC4 (Fig. 16) share a similar southwest-northeast distribution, as in the rest of the lobe complexes. The highest values are focused on the center to southern region of the outcrop, proximal to section 8; away from this point values diminish to the west and east. The orientation of the deposits in the maps share similarities with paleocurrents, although the latest are slightly more eastward.

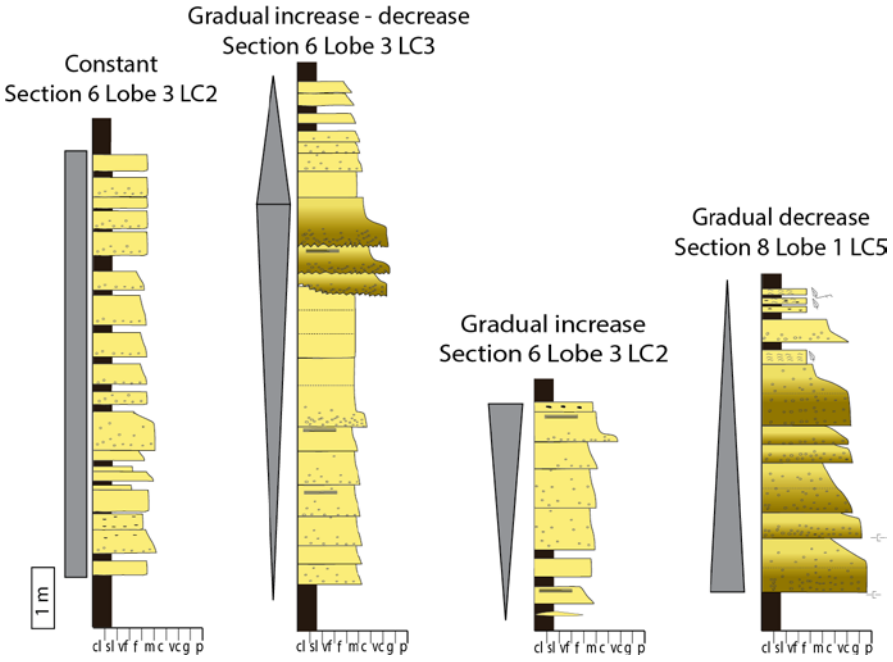

Figure 15. Types of stacking patterns recognized on the lower fan and examples from different lobes. The patterns respond to both grain size and bed thickness, although sometimes it is clearer on only one of the characteristics.

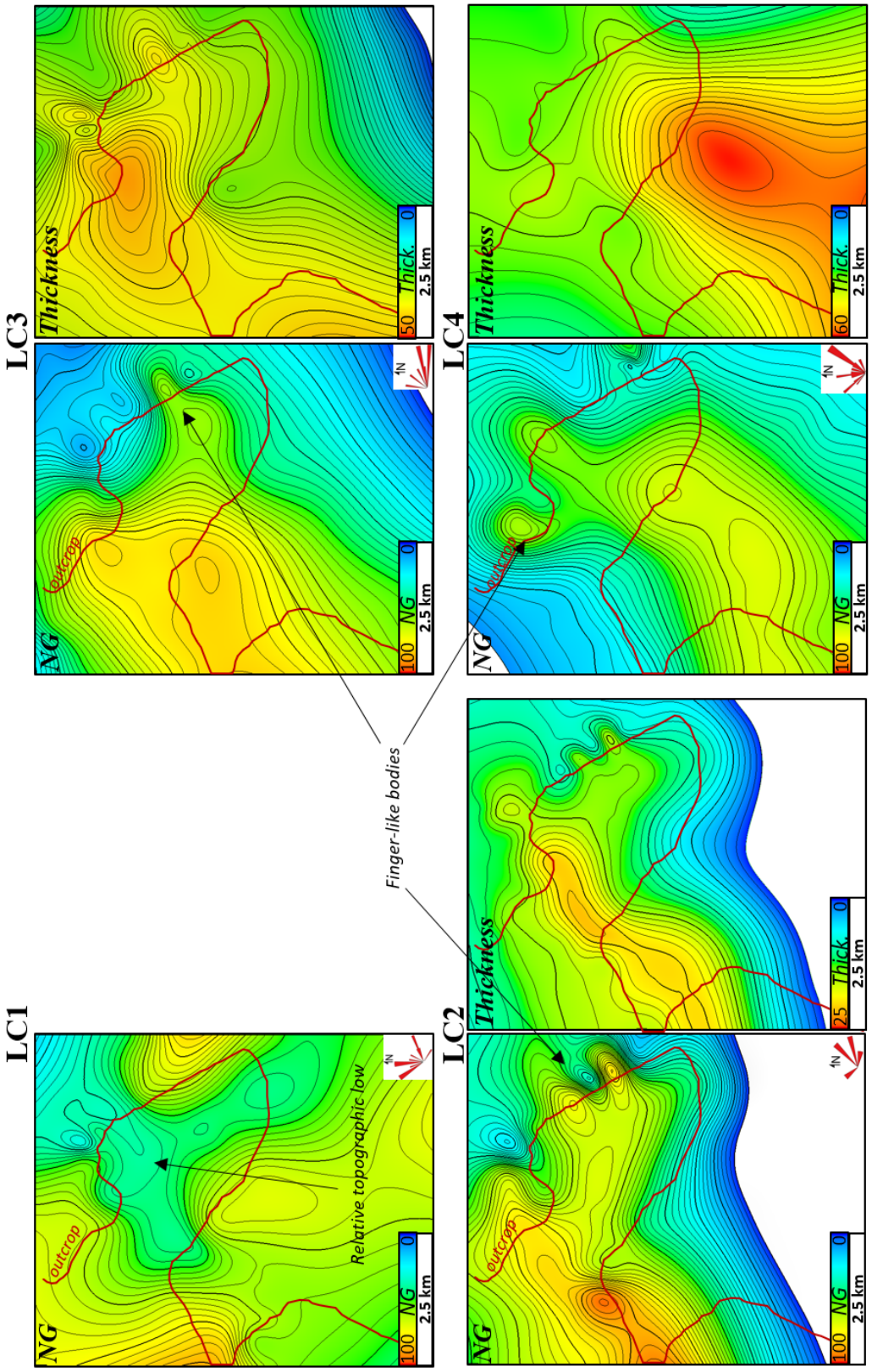
LC3
Thickness
NG
outcrop
100 NG 0
2.5 km
50 Thick. 0
2.5 km
LC4
Thickness
NG
outcrop
100 NG 0
2.5 km
60 Thick. 0
2.5 km
Finger-like bodies
LC1
NG
outcrop
Relative topographic low
100 NG 0
2.5 km
LC2
Thickness
NG
outcrop
100 NG 0
2.5 km
25 Thick. 0
2.5 km

Figure 16.

Net-to-gross (NG) and thickness maps of each lobe complex on the lower fan. Cold colors represent low values and hot colors represent high values. Paleocurrents are indicated in red at the right down corner of NG maps.

4. 2. 2. Axial variability of grain size, bed thickness, net to gross and facies

To provide a more solid description and visualization of the interpreted environments of the basin floor fan we will show how facies, grain size, bed thickness, and NG vary laterally from lobe axes to their fringe (Fig. 17). The aim of this type of analysis is to show that the qualitative interpretation made for the entire lower fan is supported by outcrop data. To focus the argument, only two lobes of LC3 will be used as an example of the methodology. Several authors have used facies and grain size distribution on deep-water settings to facilitate flow and depositional environment interpretations (Piper & Normark, 1983; Carr & Gardner, 2000; Marini *et al.*, 2011; Southern *et al.*, 2017; Spychala *et al.*, 2017; among others). Bed thickness patterns have been useful in the interpretation of depositional settings on deep-water settings (Walker & Mutti, 1973); their lateral and especially vertical arrangement had been greatly debated in the past years in publications such as Talling, 2001; Sinclair & Cowie, 2003; Clark & Steel, 2006; Bersezio *et al.*, 2009; Macdonald *et al.*, 2011; among many others. In this case, we will show frequency distributions only on different lateral sections from the same lobe units.

It is important to clarify that the measured beds on adjacent sections do not necessarily correspond exactly with each other; since there might be beds switching due to compensational stacking from one site to another.

Along depositional strike trends of lobe 3 – LC3 (Fig. 17-A)

Bed thickness histograms do not show much variation from S5 to S8. There is a slight increase from S5 to S7, with a mode increasing from 40 cm to 50 cm and a maximum value of 80 cm in S6. Grain size distribution decreases from S5 towards S8, with values ranging from upper medium – coarse sandstone in S5 to upper fine – lower medium sandstone in S8. Conglomerate beds are identified on S5 through S7. In terms of facies, there is a higher concentration of orthoconglomerates on S7 and structureless sandstones to the northwest on sections 5; these facies diminish their proportion with respect to normal graded sandstones and laminated sandstones to

the southeast. Lastly, we see NG values of 90 – 100% on sections S5 to S7 but that then diminishes to 70% on S8.

Along depositional strike trends of lobe 4 – LC3 (Fig. 17-B)

Bed thickness distribution shows a similar trend to that observed in lobe 2, with an increase in bed thickness from S5 to S7 and then diminishing towards S8. Bed thickness values range from 30 cm to 50 cm and there are fewer beds of 75 to 100 cm thickness in S5; they increase to 50-75 cm in S7 before dropping to 10 – 40 cm on S8. In terms of grain size, the trend is much more pronounced than in the previous example, with values from medium to very coarse sandstone and few conglomerates in S5 to lower medium and fine sandstones on S7 and S8. Facies also exhibit changes from northwest in S5 to southeast in S8; orthoconglomerates and structureless sandstones disappear, laminated coarse sandstone increase from S5 to S6 but then become replaced by fine laminated sandstones and normally graded sandstones. Lastly, NG does not vary much in this case, with values of 80% more or less constant throughout the panel.

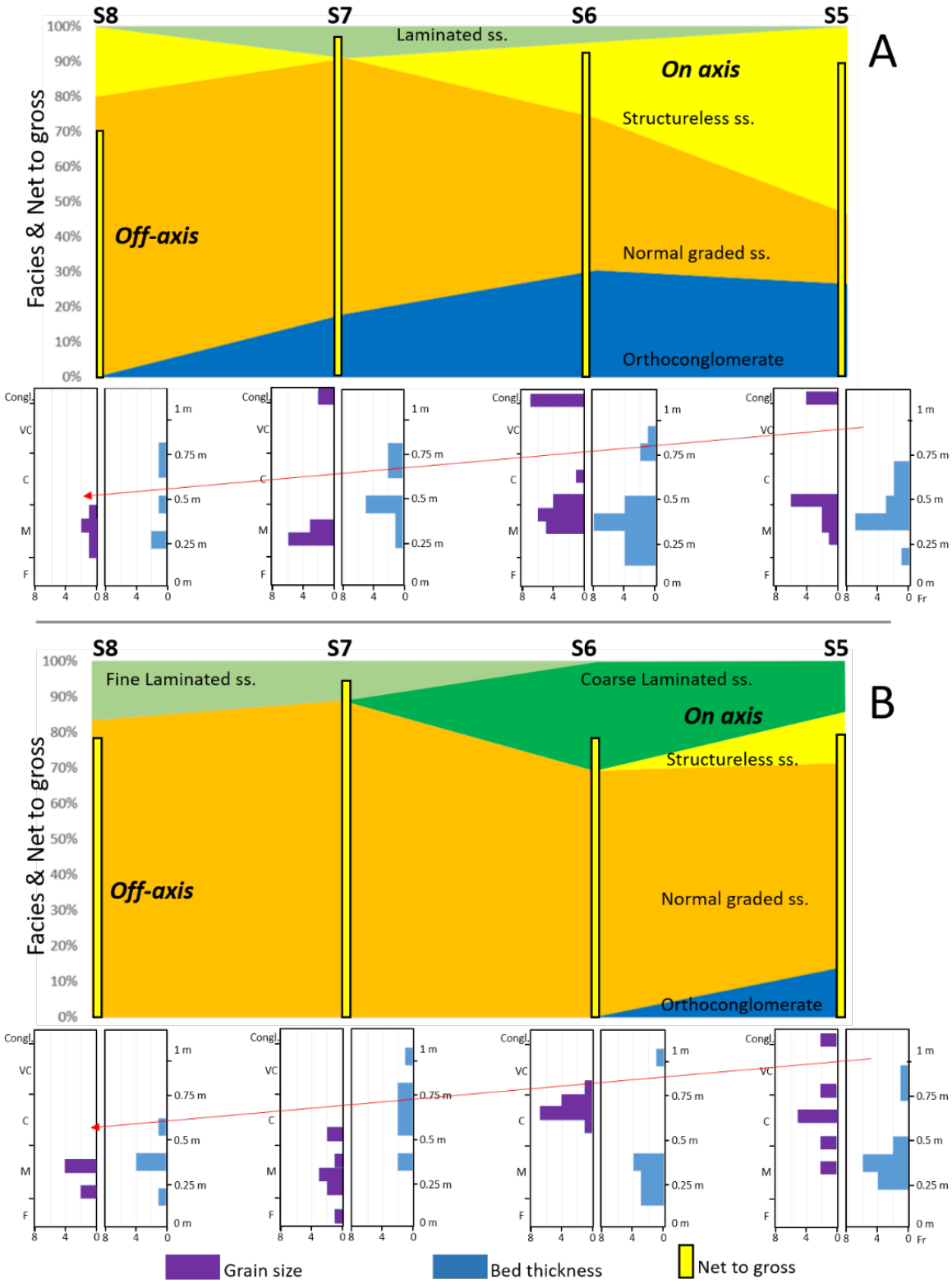

Figure 17. Facies, N/G, bed thickness, and grain size variations along strike in a correlated panel of Lobe Complex 3. A. Lobe 3. B. Lobe 4.

5. Discussion

We will first address the trends observed at lobe scale in terms of their bed thickness, grain size, facies, and NG. Next, we will discuss the controls on the lobe geometries and their vertical trends in terms of grain size and bed thickness. We will then address how the first basin floor fan in La Jardinera area evolved and provide paleogeographic reconstructions for each of the five lobe complexes. To do so, we will use the lobe complex thickness and NG maps as a framework and all measured sections with their interpreted facies associations to provide more detail. Lastly, we will discuss the role of confinement on the geometry and architecture of the basin-floor deposits.

5. 1. LOBE'S TRENDS AND AXIS VERSUS OFF-AXIS DEPOSITION

The depositional environments were interpreted at lobe scale, from axis to fringe deposits using facies, grain size, bed thickness distributions and NG (which is also an indication of the degree of amalgamation of the beds).

In lobe 3 (LC3) we interpret the axis to lie between sections 5 and 6 (Fig. 17), where we found a high proportion of high density turbidites expressed as orthoconglomerates, structureless sandstones beds and coarse grain sizes. Towards south-east, on section 8, grain size diminishes and facies associated with high density turbidity currents are replaced by low density turbidites. In terms of bed thickness, there is a very subtle decrease from section 6 towards section 8. The fact that NG diminishes from almost 100% to 70% at section 8 reinforces the idea that although we are not situated at the fringe of the lobe, we are without doubt off-axis. The type of flow responsible for the deposition of the beds of the lobe is controlled partly by the proximity to the source channels; in areas near the distributary channels the turbidity currents will have higher density and the amount of sediment allows higher amalgamation of the deposits resulting in high NG; the finer grained deposits will be dispersed laterally to more distant locations as low density turbidites (Fig. 11). This type of change in flow processes from high density turbidites in proximal settings transforming to low density turbidites away from the entry points has been registered in outcrop following the same event beds (Hirayama & Nakajima, 1977; Tokuhashi, 1989). Although in this area each individual event bed can be followed for 100's m that might be a fraction of the total length of the deposits, the same principle applies.

Lobe 4 (LC3) has a similar interpretation, although some differences arise. The axis of the lobe is interpreted to be in section 5 (Fig. 17), where we see coarser-grained deposits associated

with high density turbidites. Nevertheless, the trend in bed thickness is different than the previous example, with beds that thicken towards section 7 and then thin towards section 8. The reason for this pattern is the concentration of erosive features at sections 5 and 6, where beds were most likely thicker but where partially eroded by the next flow.

It is important to clarify that there is no simple recipe in terms of interpretation of sub-environments within a lobe using these trends, specially discussing the precise location of their axes. All the characteristics should be analyzed at the same time, and not follow only a single criterion. We have seen in lobe 4 (LC3) how a trend on its own (e.g. NG trend) can be misleading when interpreting on-axis and off-axis locations.

5.2. CONTROLS ON LOBE'S STACKING PATTERNS

For many years it has been a common assumption that coarsening and thickening-up trends and fining and thinning-up trends on lobes is an indication of progradation or retrogradation respectively (Mutti, 1974; Ricci Lucchi, 1975; Hiscott, 1981; Pickering, 1981). More recent, many of the data was reinterpreted and showed that progradational lobes owe their bed thickness patterns to 3D compensational stacking of smaller scale elements (Chen & Hiscott, 1999; Macdonald *et al.*, 2011; Prélat & Hodgson, 2013). The bed thickness patterns have to be recognized in 3D; if we see a full range of bed thickness patterns at different positions within a single lobe that are not only thickening up but also thinning up or exhibiting constant thickness at different locations, then most likely the patterns are a response to stacking of the beds due to proximity to feeder channels and compensational relief (Fig. 18, Macdonald *et al.*, 2011; Prelat and Hodgson, 2013). Macdonald *et al.*, (2011) proposed that bed-set progradation in association with aggradation leads to progressive increase in the magnitude of the flows at all parts of the system which results in increased erosion and broad erosive surfaces associated with distributary channels.

Examples of stacking patterns caused by lateral switch of bed-sets

Most of the described vertical trends of the lobes in the lower fan exhibit spatial variation (change on bed thickness trends in 100's meters), with no clear homogenous response that could indicate that the lobe is prograding or retrograding. If we consider for example lobe 5 in lobe complex 3 we can see that in panel 1 (Fig. 11) trends are fining and thinning-up in sections 5 and 6 while constant on sections 7 and 8. Downdip on panel 2 (Fig. 12), some coarsening and

thickening up sequences are observed on sections 8, 10 and 15, whereas sections 12 and 14 are fining and thinning up. If we consider only panel 1 on locations around sections 5 and 6 we might erroneously interpret these trends as a retrogradational lobe; only when we see patterns laterally and downdip, we recognize the heterogeneity of the vertical trends. We then interpret this variation in bed thickness trends as successive beds shifting laterally due to compensational stacking.

Another good example can be lobes 2 and 3 in lobe complex 2. They exhibit a coarsening and thickening up stacking pattern through the entire panel 1 (Fig. 11). Using only this panel one could argue that these trends represent a classic prograding lobe. However, on panel 2 (Fig. 12) we see that constant trends appear to be more common. Although at a proximal position we could claim a prograding stacking pattern we interpret that the lobe´s beds switch to a distal position and they aggrade with no evident progradation.

Examples of stacking patterns caused by lobe progradation/retrogradation

Lobes 2 and 3 in LC3 (Fig. 11 and 12) are the only cases in which we described coarsening and thickening-up or fining and thinning-up stacking patterns on all or almost all of the locations where sections were measured.

Lobe 2 shows, on panel 1 and 2 (Fig. 11 and 12) coarsening and thickening-up trends through almost all locations with the exception of section 8, panel 1 where the top is thinning up and section 8, panel 2, where there is no clear trend. Since the trends are well observed across most of the entire area we interpret a prograding trend of the lobe.

Lobe 3 is the most complex lobe, with multiple erosive features and several trends and variations in grain size and thickness. However, we identify an overall coarsening and thickening-up followed by fining and thinning-up trend for the entire lobe both on panel 1 and 2 (Fig. 11 and 12). The increasing number of erosive features on the vertical trend as the coarsening-up trends are a good indication that the lobe was formed by prograding from unconfined to channelized beds, which then retrograde, going back to an unconfined scenario with thinner and finer grained beds.

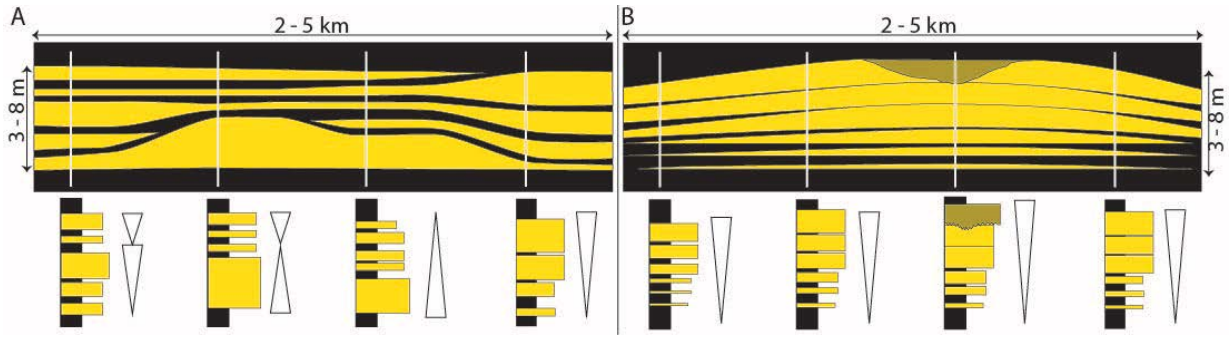

Figure 18. Diagram showing changes in accumulation of sand and mud on a vertical profile. Diagram A shows the origin of compensation patterns, note how thickness trends vary across the lobe. Thinning and thickening-up trends are observed together with regions of no thickness variation. Diagram B shows the thickening-up trends generated by prograding beds. Trends are observed through the entire lobe, and are interrupted only by localized erosion generated by bypass surfaces and channels. Modified from Macdonald *et al.*, 2011.

5. 3. STRATIGRAPHIC EVOLUTION OF THE LOWER FAN

The exposures of Los Molles Fm. described in the La Jardinera area represent the first basin floor fan of a new shelf-slope-basin floor system, formed by overall aggradational lobe complexes that are characterized mostly by aggradational and to a lesser extent by progradational lobes. Although the lower fan varies spatially, its total thickness on the area is about 150–200 m; it is sand rich on a proximal setting (panel 1, Fig. 11) with values that range from 70 – 80% at the lobe complex scale. It is characterized by changes in facies architecture and depositional settings at a lobe scale, responding to the types of flows that run through the entry points to the basin floor. Although mostly unconfined geometries are recognized it is important to emphasize the presence of distributary channels on this basin floor setting (Fig. 9C and 10), since they are responsible for the lobe's final geometry and sediment dispersal characteristics.

Analysis of the basin geometry during late Triassic – early Jurassic times by different authors (e.g. Vergani *et al.*, 1995, 2005; Morabito, 2010) have indicated that the base of Los Molles Fm. was still under the influence of late-stage rifting. This resulted in thickness variations related to measured positions within the hemigrabens; these geometries can be observed easily on seismic images (Fig. 4). In la Jardinera area, the westernmost fault oriented southeast–northwest

called Rahue Fault (Fig. 3 and 5 A) has been described by Morabito (2010), suggesting that the entire area of interest sits on a hemigraben.

The lower fan succession begins with the deposits interpreted as **lobe complex 1** (LC1, Fig. 19-A). LC1 is the only lobe complex that exhibits 2 different paleocurrent directions, one to the east-northeast and another to the northwest (Fig 5B and 11). Although further analysis should be made regarding the geometry of the basin at this earliest stage of Los Molles Fm. in La Jardinera area, we interpret the paleocurrents as reflecting the heterogeneities on the basin floor at the onset of coarse-grained infilling. Paleocurrents towards the northwest are following the main orientation of Rahue fault, while paleocurrents towards the east–northeast are transversal to it (Fig 5A). This pattern can be observed on NG maps (Fig. 16), where deposits seem to be following a southeast – northwest distribution on the southern part of the map, and a west-east distribution on the northern part. This interpretation is in accordance with the suggestion of Burgess *et al.* (2000), who stated that the complex faulted topography during Pliensbachian-Toarcian times was an important control on the dispersal patterns of gravity flows into the basin.

LC1 is composed of 2 lobes formed mainly by unconfined elements that show an aggradation pattern. These lobes are separated by a fine-grained interval with a high concentration of debris flows with slumped features at the northwest on panel 1.

It is difficult to discern a clear pattern of sedimentation on LC1 because paleocurrents have variable directions. This resulted in lack of clear trends in facies associations, with no obvious lobe axis and with distributary channels occurring at different positions on the lobe complex.

Figure 19-A shows the interpreted paleogeographic reconstruction for LC1. Although 2 systems are drawn on the figure this is only for representation of the different routing systems and not necessarily indicating that there are 2 recognizable systems clearly separated.

Lobe complex 2 (LC2, Fig. 19-B) is sitting on top of LC1 with its main axis oriented southwest–northeast according to the NG map and total thickness map and in alliance with paleocurrents that have similar orientation (Fig. 16). If we consider the NG map of LC1 to represent not only sand distribution but local topography left by its deposits, LC2 main axis occupies a position that could be considered a low, with higher NG and thickness values near sections 4 on panel 1 (Fig. 11). Three lobes compose this lobe complex, that firstly onlaps LC1 towards southeast (Fig. 11) and then aggrades. Although lobes 2 and 3 might show coarsening and thickening up trends on panel 1 they do not represent prograding lobes, since these trends are not

seen in downdip areas. The lobes of LC2 are mainly formed by unconfined compensationally stacked lobe elements and small distributary channels sitting on top. The geometry of the lobe complex seen on the maps is similar to what authors like Bouma & Rozman (2000), Rozman *et al.* (2000), Groenenberg *et al.* (2010), Spychala *et al.* (2017), have referred to as finger-like sandstone bodies. These terminations can be misleading and may be interpreted as channelized features (e.g van der Werff & Johnson, 2003). In this case, we interpret these geometries to be a response of focused sediment dispersal associated with high density turbidity currents on channel to lobe transitions. Flows that reached the fringe of the lobe complex had a narrow lateral extent and deposited stretch finger-like beds with high side relief (Groenenberg *et al.*, 2010).

A fine-grained interval of 1 – 5 m thick separates **Lobe Complex 3** (LC3) from LC2. According to NG and thickness maps (Fig. 16), LC3 main axis has a similar orientation to that of LC2 (southwest-northeast), although the measured paleocurrents have a more eastward direction (Fig. 19-C). We observe a high level of aggradation from LC2 to LC3 at a lobe complex scale with no major changes on the location of its main axes. However, the deposits broaden and occupy a larger area both laterally and longitudinally. LC3 on panel 1 (Fig. 11) exhibits the highest proportion of proximal facies association associated with distributary channels and on-axis amalgamated lobe deposits. This could be interpreted as a relative progradation of the system at a lobe complex scale, however, the NG map shows that the amount of sand being delivered basin ward is not higher than in LC2 and it is focused on particular locations, exhibiting again a fingerlike body geometry. Contrary to LC2, this elongated features on the maps are a direct response to distributary channels with high proportion of conglomerates and coarse sandstone that reach the outer part of the lobe complex.

LC3 is composed of 6 highly amalgamated and aggradational lobes with little change in the location of the lobe's axis, as seen in sections 5 to 7 on panel 1 (Fig. 11). Lobe 1 and 6 are composed exclusively by unconfined elements, but lobes 2 to 5 present distributary channels on their axis. These channels do not remain on the same location from lobe to lobe, they shift laterally towards the northwest (Fig. 11), giving evidence that lobes do not only aggrade but also shift laterally. As we pointed out in the previous sections, most of the lobes exhibit spatially varied grain sizes and bed thickness trends that respond to compensational stacking of the beds and proximity to feeder channels. However, the few cases where lobe progradation does occur is interpreted to happen on lobe complex 3 (lobes 2 and 3).

Lobe 3 on LC3, might represent one of the best examples of channel to lobe transition on the area. It shows the change from unconfined beds that thicken and coarsen-up until erosive bases and conglomerates appear. These erosion surfaces are not as deep as those found on slope channels or very proximal channels on the basin floor (locally can be up to 2.5 m). The erosions are 100's m wide and associated with relatively few event beds (up to 5) that can be traced laterally. These shallow depressions are sometimes filled by the same flow responsible for the erosion; pattern recognized by other authors like Cazzola *et al.*, (1981), who studied channel to lobe transition zones of the Roccetta Formation on the Piedmont Basin, Italy. On top of the erosive and conglomeratic beds, continuous and tabular geometries are found; grain size diminishes and beds thin-up. Several of the channels seen on the lobes on panel 1 (Fig. 11) are represented downdip (panel 2, Fig. 12) by thinner, finer grained and lower NG unconfined bed-sets. The close relation between confined and unconfined events, the broad nature of the erosive bases and changes in grain size found on few meters on the vertical trend of hundreds of meters on a downdip lateral trend is a very good indication that the system is at a channel to lobe transition (Mutti & Normark, 1987, 1991; Kostrewa, 2004).

Lastly, there is a shift towards the southeast on the axis from LC3 to **Lobe Complex 4** (LC4, Fig. 19-D). NG and thickness maps indicate a distribution elongated south southwest – north northeast with similar paleocurrent directions. The main axes most likely shifted to the south due to compensational stacking; LC3 must have left a relative topographic high causing the system to move towards the south.

LC4 is composed of 6 aggradational lobes that are interpreted to have the depositional axis on section 8, panel 1 (Fig. 11). However, and opposite to the rest of the lobes on the panels, no channelized features are recognized. Each lobe is composed by unconfined compensationally stacked bed-sets.

As in LC2 and LC3, some fingerlike geometries are recognized on the maps, in this case evidenced by sand distribution on the NG map. As previously stated, these geometries are a response to high density narrow flows that generated elongated morphology downdip.

The lack of distributary channels on the panels, along with lower NG and total thickness values downdip is an indication that the lateral shift was accompanied by a backstep of the system.

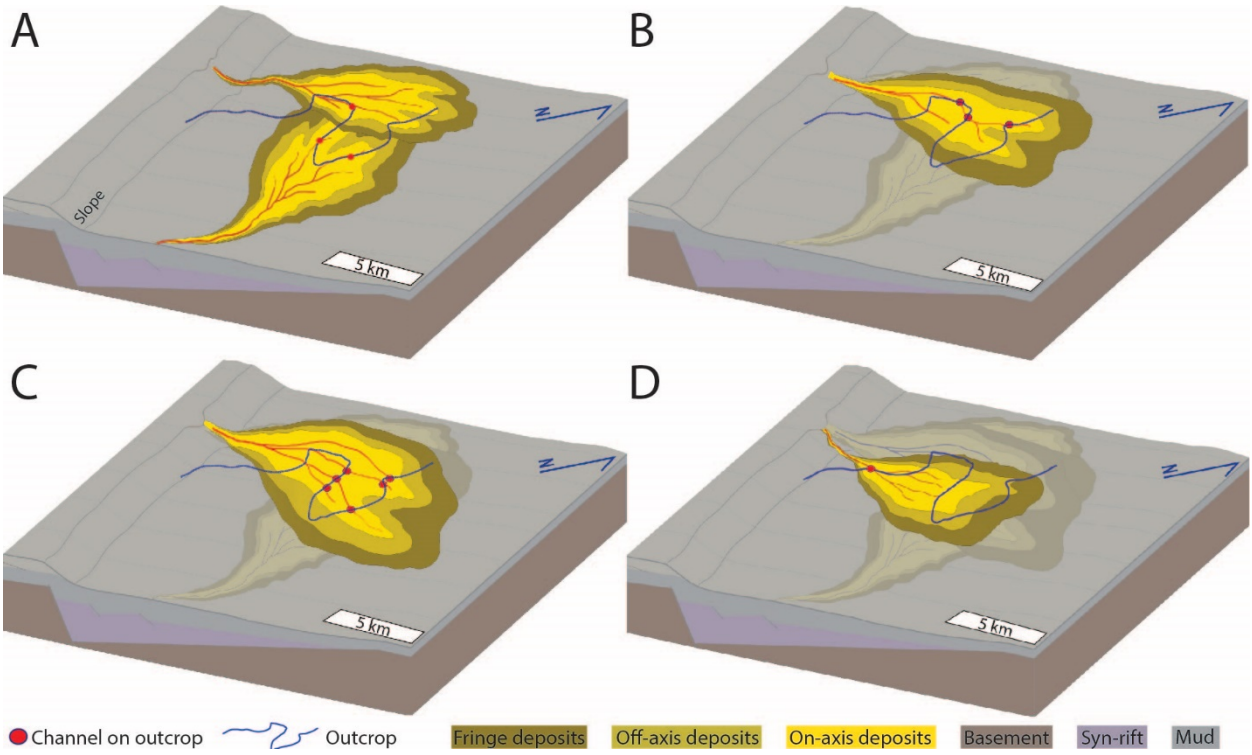

Figure 19. Paleogeographic reconstructions of the lobe complexes forming the lower fan. Each lobe complex is represented here with on-axis to off-axis and fringe deposits moving away from the main sediment entry points. Note that the shape of the lobe complexes is not perfectly lobated but that it has serrated borders (see discussion. The channels that are interpreted on outcrop (red line) are marked here as blue dots. A hemigraben is represented on the block diagrams as a possible structural setting for the base of Los Molles Fm.

5. 4. TYPE OF STACKING AND ROLE OF TOPOGRAPHY AND CONFINEMENT ON THE BASIN FLOOR

Many of the studies on deep-water sedimentation and the influence of topography on confinement vs unconfinement on their deposits were carried out on outcrops where the limits of the basin is well known and onlap relationship exists and can be seen between the deposits and the basin border (e.g., Pickering & Hiscott, 1985; Felletti, 2002; Sinclair & Tomasso, 2002; Cornamusini, 2004; Smith, 2004; Tinterri & Piazza, 2018).

One of the difficulties regarding Los Molles Fm. interpretation of topography influence on the basin floor gravity flows is due to the fact that there are no clear large scale onlap surfaces of the deep-water sediments against the borders of the basin. Consequently, we cannot know for sure if at the time of Molles Fm. the basin was partitioned and acting as a single hemigraben depocenter,

or if it was connected with other parts of the basin. Confinement is a relative term, since it is actually dependent by the incoming flow characteristics (height, volume, concentration) and the recipient (basin) topography. This means that even if it was an isolated hemigraben at the time of deposition, the flows might not have covered the entire area and so the system was still unconfined.

To evaluate the influence of confinement in the area, facies, thickness and stacking patterns need to be used and work backwards towards the flow processes. Several authors have documented the importance of flow confinement as a control of sediment dispersal and stacking patterns at different scales, from beds to lobe complexes (e.g., Pickering & Hiscott, 1985; Lomas & Joseph, 2004; Smith, 2004; Macdonald *et al.*, 2011; Marini *et al.*, 2011, 2015; Southern *et al.*, 2015). Other authors, like Bouma (2004), have stressed the idea that confined basins tend to be relatively coarse-grained, with a significant amount of gravel and a low percentage of fine-grained material.

In unconfined to semi-confined settings, the dominant manner of stacking of single beds and lobes is dominantly compensational (Marini *et al. 2015*, Fig. 20). This suggests that lenticularity of lobe stacks results from compensation of successive event beds. The arrangement of unconfined to semi-confined lobes and lobe complexes is thus reflected in lateral variations of net to gross, thickness and facies in response to auto-cyclical controls of depositional topography (Marini *et al.* 2015).

On the other hand, confined lobes (as described and interpreted by Marini *et al.*, 2011, 2015) show an arrangement of beds that is dominantly aggradational with flat three-dimensional geometries in response to flow ponding. As a result, component units pile up vertically (vertical stacking), compensational processes are unimportant and the final architecture of confined lobes is sheet-like, with basin-wide extensive lobe stacks that shale out and pinch out toward basin margins (Fig. 20).

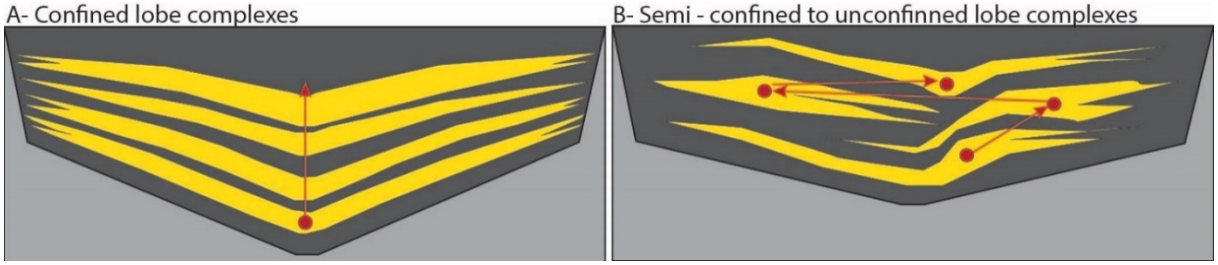

Figure 20. Simplified diagram showing the stacking pattern of lobes in confined (a) and semi-confined (b) lobe complexes along depositional strike. The red arrows show the probable trajectory of the center of mass of lobe sets (i.e. the locus of main sand deposition). Modified from Marini *et al.*, 2015. No scale intended.

The lower fan deposits analyzed in La Jardinera area show compensational stacking patterns at a bed scale that is translated up to lobes and lobe complexes, where we observe that lobe complex or lobe axis does not remain fixed at a certain location but shifts laterally (Fig. 11). However, a marked amount of aggradation is observed at lobe and lobe complex scale. We described in previous sections how LC2 filled topographic lows left by LC1 (Fig 11 and 16). From LC2 to LC3 there is a high level of aggradation to a point when the fan could not continue to construct vertically and an auto-cyclic response shifted the feeder channels towards the south on LC4. LC3 also presents good evidence of lateral compensation of its lobes while aggrading, with the axis of the lobes migrating towards the northeast (Fig. 11).

The above-mentioned descriptions on how deep-water sediment at different hierarchical scales stacked together in La Jardinera area seems to point to an unconfined setting. However, LC1 might reflect a certain influence from inherited structures of rift. The bipartite paleocurrents (northwest and northeast) are parallel and transversal to the main fault of the hemigraben interpreted on the area (Rahue fault, Fig. 5A) and they could have acted as preferential sediment routes. What is more, beds on LC1 appear to be relatively continuous with couplets of sand – mud, possibly reflecting a response to significant confinement on the basin floor due to ponding. Future work could focus on an analysis of the lower-most portion of the fan to generate detailed bed correlations in order to test this hypothesis.

5. 5. COARSE GRAINED FAN MODEL

The basin floor fan of La Jardinera area has most of the general features associated with coarse-grained submarine fans (Reading & Richards, 1994; Bouma, 2000). Net to gross is very

high, almost 100% in the axes of some lobe complexes; average grain size is medium to coarse grained sand; they have relatively small dimensions, 8 km width on average; and they stack vertically, with no major lateral shifts. However, there are some characteristics that might have been overlooked due to the lack of laterally extensive and vertically continuous outcrops, such as the variation of facies laterally, the architecture of the deposits and geometries of the sandstone bodies downdip. On figure 21 we describe the new model for coarse-grained deep-water fans through comparison with one from Reading & Richards (1994); in addition we combine outcrop detailed facies analysis with seismic from modern coarse-grained fans (Deptuck *et al.*, 2008) to understand how the basin-floor fan architecture responds to bedset-scale processes.

Bed architecture variability that exists at a lobe scale is reflected on higher hierarchies within the fan. Near the apex of the lobe, grain size is greater and NG is higher, diminishing to the fringes. These trends are reflected in facies variation; distributary channels near the axis of the system, deposited high density turbidity currents that dissipated laterally into more dilute flows. Consequently, it is worth noticing that although sandy rich systems might be dominated by high density turbidity currents, changes in flow along the axis or lateral to the axis are likely to occur, along with variations on grain size and NG. Trends evaluated at a lobe scale can be extrapolated to the whole lobe complex, and eventually to the scale of the entire fan (Figs. 21 A and C).

Lobe complex size on the fan is relatively small compared to muddy systems (Bouma, 2000). However, the overall fan shape might not be radial but elongated (Fig. 21 A and B); see also the thickness maps of individual lobe complexes of figure 16. From thickness maps and bedding correlations, we estimate an average width of 9 km and a length of approximately 20 km for lobe complex scale. In addition, the geometry of the system along downdip is not lobate but it presents elongated features previously referred to as finger-like sandstone bodies (Fig. 21 A). These features are a response to channelized flows and / or to focused sediment dispersal and high relief unconfined deposits.

Compensational stacking plays a major role in the vertical and lateral arrangement of the different elements within the coarse-grained basin-floor fan of Los Molles Fm. (Fig. 11). The topography inherited by previous deposits of the fan function as preferential sinks; as clearly seen on LC2 over LC1 (Figs. 11 & 16). In addition, progradational vs retrogradational stacking patterns at lobe complex scale is subtle and difficult to map. The systems aggrade and follow preferential routes for sediment dispersal, prograding only a minor distance.

Studies from the East Corsica in the Golo Fan (Deptuck, 2008) portrayed the geometry of a coarse-grained deep-water system at a lobe complex scale. The architecture of one of the Golo lobe complexes imaged on seismic resembles that of some of the lobe complexes on this outcrop study, showing how lobes are compensationally stacked and how new deposits follow preferential paths between previous lobe deposits (Fig. 21 C). While the general architecture is clearly seen on seismic there is still lack of data at facies detail. On figure 21 C, we combine schematic logs with their seismic interpretation; logs show the facies we might expect to see as recognized in the outcrop study. High density turbidites and channelized high-density turbidites can be expected on the axis of the lobes where they are thicker. To the sides, grain size diminishes, beds are thinner and less amalgamated, resulting on lower NG (Fig. 16). Facies are most commonly associated with more dilute turbidites on the margins of each of the lobes. The distribution of the channels is controlled mainly by the aggradation of the lobes. Bedsets aggrade to a point from which they cannot continue to build vertically. This promotes up-dip avulsion of the channels which will preferentially follow the topographic low lateral to the aggraded beds. The channel (turbidite flows) will then be forced to migrate laterally, cutting through previous deposits (see changes on individual lobe's axis position on Fig. 21 C).

5. 6. APPLICATIONS TO RESERVOIRS IN THE SUBSURFACE

Cuyo Gr (in particular Los Molles Fm.) has been a reservoir/source rock of interest for many years since it comprises a proven petroleum system (Cruz *et al.*, 1999; Cruz, 2002; Gómez Omil *et al.*, 2002; Villar *et al.*, 2005; Legarreta *et al.*, 2008). However, only during the past 5 years has special attention been paid to the possibility of an emergent play called basin centered gas systems or "BCGS" (Raggio *et al.*, 2014; Omil & Borghi, 2017). This type of play consists of regional accumulations that are gas saturated, abnormally pressured, commonly lack a downdip water contact and have low permeability reservoirs (Law, 2002). Los Molles Fm. has the potential to hold major gas resources in Neuquén Basin associated with low porosity-permeability sandstones deposited by gravity flows on basin floor fans and slope channels (Raggio *et al.*, 2014; Omil & Borghi, 2017).

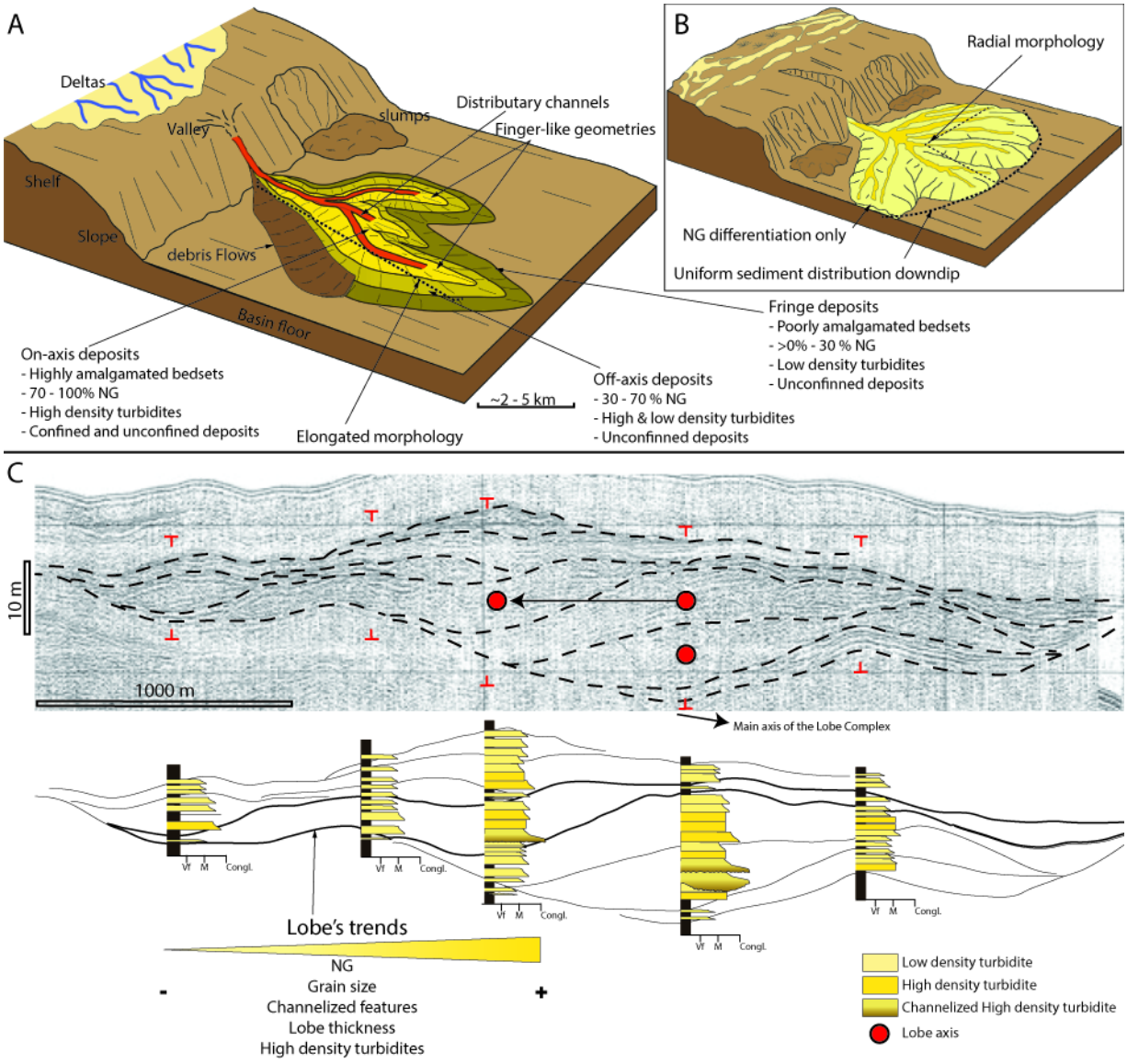

Figure 21. A- Depositional model for coarse-grained deep-water fans. B- Previous depositional model for coarse-grained systems modified from Reading & Richards, 1994. Main differences in new model are listed in the box. C- Seismic interpretation from Deptuck *et. al.*, (2008) and schematic logs showing possible main facies assemblage using outcrop model from this study.

The outcrops of La Jardinera area allow a 3D visualization of the potential reservoirs, probably the best outcrop example anywhere in the basin. Seismic analysis, along with drilling decisions should be accompanied by proper paleogeographic reconstructions, considering the lateral and vertical variations we described in previous chapters. The entire fan (which is approximately 150-200 m thick) should be visible on seismic; however, lobe complexes and single

lobes might represent sub-seismic features that cannot be detected (unless seismic data has high frequencies of 60-80 hz; Marini *et al.*, 2015). Heterogeneities at this scale can be interlobe complexes or interlobe shales that should be identified as they can compartmentalize potential reservoirs. Information such as trends in NG, degree of amalgamation of single beds and lobe elements, bed thickness, and grain size patterns are easily obtained from wells. The distribution of these characteristics, such as we observe in outcrop, allows predictions to build a subsurface model and thus diminish risk for drilling projects.

The analysis methodology of the basin floor fans in La Jardinera can also be applied to other deep-water, coarse-grained systems elsewhere. We consider that the key aspects to consider when evaluating this type of deposits are:

1- Proximity to the axis of the system: at proximal to medial settings, the closer to the axis of the fan the higher the net to gross and the degree of amalgamation at different scales. For example, Lobe complex 3 defined in this study would be the ideal case with very high net to gross and almost complete amalgamation of its lobes on panel 1 (Fig 11).

2- Geometry downdip: although most of the deposits are considered unconfined, classic lobate shapes have been proven incorrect in reality, and elongate, serrated terminations are more common. This means that downdip of the system, pinch outs will not occur homogenously and the coarse material will be focused in particular areas.

6. Conclusions

The aim of this study was to (1) provide an enhanced model for coarse-grained basin-floor fans, (2) increase the understanding of the Los Molles Fm. by delivering the first detailed paleogeographic reconstructions of probably the first basin floor fan in the Neuquén Basin and (3) to provide reservoir analogs for subsurface exploration. These goals required facies analysis, identification of geometries and architecture of the deposits at different hierarchical levels, interpretation of lateral trends in terms of facies, grain size, bed thickness and net to gross, and bed thickness and grain size analysis of vertically stacked successions.

The lower Los Molles Fan is composed of 4 lobe complexes (each averaging 40 m thick) separated by fine grained intervals (4 m thick in average). Each lobe complex is composed of 2 to 6 lobes (each averaging 5 m in thickness) that are formed mainly by unconfined bedsets, although distributary channels were identified and play and important role throughout the succession. LC1

exhibits 2 different paleocurrent directions and a NG distribution that might reflect basin floor topography imposed by syn-rift structures. LC2 is located on topographic lows remnant from LC1 with its axis elongated southwest–northeast, with similar paleocurrent directions; it is composed by 3 aggrading lobes that present unconfined, compensationally stacked bed-sets and small distributary channels on their top. LC3 aggraded on top of LC2 with a similar northeasterly axis orientation, although deposits broaden and occupy a larger area. It is composed of 6 aggrading lobes that are highly amalgamated along the axis. These lobes also support the highest proportion of distributary channels. LC4 shifts towards the southeast and backsteps. It is composed of 6 aggradational lobes with unconfined deposits.

Vertical trends of bed thickness observed in 3D indicate that only lobes 2 and 3 from LC3 exhibit consistent coarsening and thickening-up or fining and thinning- up stacking patterns across the area. The increasing number of erosive features along with the trends themselves is an indication of prograding and retrograding of lobes where most proximal facies are associated with amalgamated erosive features.

The deposits of the lower fan show compensational stacking through the succession and these are likely to be autocyclic responses of the growing system in an unconfined setting. Though LC1 might be reflecting 2 different sediment routes that are associated with an initial complex geometry inherited from the rift.

A new model for coarse-grained deep-water fans was proposed. The main characteristics rely on variability from the axis to the fringe of the system. On-axis, lobes are thicker, there is higher proportion of channels and high density turbidites, thicker beds and high NG and grain size. Towards the fringe, lobes are thinner, there is higher proportion of low density turbidites, thinner beds and lower NG and grain size. In addition, the morphology of the lobe complexes is markedly elongated and they present finger-like sandstone geometries downdip associated with distributary channels.

Lastly, the outcrops of La Jardinera allow a good characterization of turbidite deposits that can be applied to reservoirs in the subsurface and give hints on how to make paleoenvironmental interpretations where data is scarce and widely spaced. Particular features to consider when analyzing these rocks on the subsurface are: (1) the proximity to the axis of the system; this will give higher NG and amalgamation of lobes that translates into fewer shale heterogeneities that

could compartmentalize the reservoirs. (2) the geometry of the lobe complexes downdip is elongated and serrated, and sand pinchouts might not occur homogenously.

Bibliography

Arregui, C., **Carbone, O.** and **Martínez, R.** (2011) El Grupo Cuyo (Jurásico Temprano-Medio) en la cuenca neuquina. *Relat. del XVIII Geológico Argentino Geol. y Recur. Nat. la Prov. del Neuquén*, 77–89.

BAAS, J.H. (1994) A flume study on the development and equilibrium morphology of current ripples in very fine sand. *Sedimentology*, **41**, 185–209.

Baas, J.H., **Best, J.L.** and **Peakall, J.** (2011) Depositional processes, bedform development and hybrid bed formation in rapidly decelerated cohesive (mud-sand) sediment flows. *Sedimentology*, **58**, 1953–1987.

BERSEZIO, R., **FELLETTI, F.**, **RIVA, S.** and **MICUCCI, L.** (2009) Trends in Bed Thickness and Facies of Turbiditic Sandstone Bodies: Unravelling the Effects of Basin Confinement, Depositional Processes, and Modes of Sediment Supply. *Extern. Control. Deep. Depos. Syst.*, 303–321.

Bouma, A.H. (1962) Sedimentology of Some Flysch Deposits: A Graphic Approach to Facies Interpretation. Elsevier, Amsterdam/New York 168.

Bouma, A.H. (2004) Key controls on the characteristics of turbidite systems. *Geol. Soc. London, Spec. Publ.*, **222**, 9–22.

Bouma, A.H. (2000) Coarse-grained and fine-grained turbidite systems as end member models: Applicability and dangers. *Mar. Pet. Geol.*, **17**, 137–143.

Bouma, A.H. and **Rozman, D.J.** (2000) AAPG Memoir 72/SEPM Special Publication No. 68, Chapter 25: Characteristics of Fine-Grained Outer Fan Fringe Turbidite Systems.

Bowen, A.J., **Normark, W.R.** and **Piper, D.J.W.** (1984) Modelling of turbidity currents on navy submarine fan. *Sedimentology*, **31**, 169–185.

Burgess, P.M., **Flint, S.** and **Johnson, S.** (2000) Sequence stratigraphic interpretation of turbiditic strata: An example from Jurassic strata of the Neuquén basin, Argentina. *Bull. Geol. Soc. Am.*, **112**, 1650–1666.

Camacho, H., **Busby, C.J.** and **Kneller, B.** (2002) State Beach , California. *Am. Assoc. Pet. Geol. Bull.*, **86**, 1543–1560.

Carr, M. and **Gardner, M.H.** (2000) Portrait of a basin-floor fan for sandy deepwater systems, Permian Lower Brushy Canyon Formation, West Texas. *AAPG Mem.*, **72**, 215–231.

Cazzola, C., **Fonnesu, F.**, **Mutti, E.**, **Rampone, G.**, **Sonnino, M.** and **Vigna, B.** (1981) Geometry and facies of small, fault-controlled deep-sea fan systems in a transgressive depositional setting (Tertiary Piedmont Basin, Northwestern Italy). In: *Excursion guidebook of the 2nd European regional meeting of the International Association of Sedimentologists*, 5–56.

Cazzola, C., **Mutti, E.** and **Vigna, B.** (1985) CHAPTER 26 Cengio Thrbidite System, Italy.

Chen, C. and **Hiscott, R.N.** (1999) Statistical Analysis of Turbidite Cycles in Submarine Fan Successions: Tests for Short-Term Persistence. *J. Sediment. Res.*, **69**, 486–504.

Clark, B.E. and **Steel, R.J.** (2006) Eocene Turbidite-Population Statistics from Shelf Edge to Basin Floor, Spitsbergen, Svalbard. *J. Sediment. Res.*, **76**, 903–918.

Cornamusini, G. (2004) Sand-rich turbidite system of the Late Oligocene Northern Apennines foredeep: physical stratigraphy and architecture of the 'Macigno costiero' (coastal Tuscany, Italy). *Geol. Soc. London, Spec. Publ.*, **222**, 261–283.

Cronin, B., **Owen, G.**, **Hartley, A.** and **Kneller, B.** (1998) Slumps, debris flows and sandy deep-water channel systems: implications for the aaplication of sequence stratigraphy to

deep water clastic sediments. **155**, 429–432.
Cruz, C. (2002) Hábitat de hidrocarburos y sistemas de carga los molles y vaca muerta en el sector central de la cuenca neuquina. Argentina. *V Congr. Explor. y Desarro. Hidrocarburos*, 1–20.
Cruz, C.E., **Robles, F.**, **Sylwan, C.A.** and **Villar, H.** (1999) Los sistemas petroleros jurásicos de la Dorsal de Huincul, Cuenca Neuquina, Argentina. In: *Congreso de Exploración y Desarrollo de Hidrocarburos*, 177–195.
Deptuck, M.E., **Piper, D.J.W.**, **Savoye, B.** and **Gervais, A.** (2008) Dimensions and architecture of late Pleistocene submarine lobes off the northern margin of East Corsica. *Sedimentology*, **55**, 869–898.
Felletti, F. (2016) Depositional architecture of a confined, sand-rich submarine system: The Bric la Croce-Castelnuovo turbidite system (Tertiary Piedmont Basin, Oligocene, NW Italy). *Ital. J. Geosci.*, **135**, 365–382.
Felletti, F. (2002) Complex bedding geometries and facies associations of the turbiditic fill of a confined basin in a transpressive setting (Castagnola Fm., Tertiary Piedmont Basin, NW Italy). *Sedimentology*, **49**, 645–667.
Franzese, J., **Spalletti, L.**, **Pérez, I.G.** and **Macdonald, D.** (2003) Tectonic and paleoenvironmental evolution of Mesozoic sedimentary basins along the Andean foothills of Argentina (32°-54°S). *J. South Am. Earth Sci.*, **16**, 81–90.
Franzese, J.R. and **Spalletti, L.A.** (2001) <late triassic-early Jurassic.pdf>.
Gervais, A., **Mulder, T.**, **Savoye, B.** and **Gonthier, E.** (2006a) Sediment distribution and evolution of sedimentary processes in a small sandy turbidite system (Golo system, Mediterranean Sea): Implications for various geometries based on core framework. *Geo-Marine Lett.*, **26**, 373–395.
Gervais, A., **Savoye, B.**, **Mulder, T.** and **Gonthier, E.** (2006b) Sandy modern turbidite lobes: A new insight from high resolution seismic data. *Mar. Pet. Geol.*, **23**, 485–502.
Gervais, A., **Savoye, B.**, **Piper, D.J.W.**, **Mulder, T.**, **Cremer, M.** and **Pichevin, L.** (2004) Present morphology and depositional architecture of a sandy confined submarine system: the Golo turbidite system (eastern margin of Corsica). *Geol. Soc. London, Spec. Publ.*, **222**, 59–89.
Gómez Omil, R.G., **Schmithalter, J.**, **Cangini, A.**, **Albariño, L.** and **Corsi, A.** (2002) El Grupo Cuyo en la Dorsal de Huincul: consideraciones estratigráficas, tectónicas y petroleras, Cuenca Neuquina. In: *V° Congreso de Exploración de Hidrocarburos*,
Groenenberg, R.M., **Hodgson, D.M.**, **Prelat, A.**, **Luthi, S.M.** and **Flint, S.S.** (2010) Flow-Deposit Interaction in Submarine Lobes: Insights from Outcrop Observations and Realizations of a Process-Based Numerical Model. *J. Sediment. Res.*, **80**, 252–267.
Grundvåg, S.A., **Johannessen, E.P.**, **Helland-Hansen, W.** and **Plink-Björklund, P.** (2014) Depositional architecture and evolution of progradationally stacked lobe complexes in the Eocene Central Basin of Spitsbergen. *Sedimentology*, **61**, 535–569.
Gulisano, C. and **Gutierrez Pleimling, A.** (1994) Field trip guidebook, Neuquina Basin, Mendoza Province. In: *Fourth International Congress on Jurassic Stratigraphy and Geology*,
Gulisano, C., **Gutierrez Pleimling, A.** and **Digregorio, R.E.** (1984) Esquema estratigráfico de la secuencia jurásica del oeste de la provincia del Neuquén. In: *Congreso Geologico Argentino. No. 9*, 236–259.
Hampton, M.A. (1972) The role of subaqueous debris flow in generating turbidity currents. *J.*

Sediment. Petrol., **42**, 775–793.
Haq, B., **Hardenbohl, J.** and **Vail, P.R.** (1987) Chronology of fluctuating sea levels since the Triasic (250 million years ago to present). *Sci. York*, **23**, 1156–1167.
Haughton, P., **Davis, C.**, **Mccaffrey, W.** and **Barker, S.** (2009) Hybrid sediment gravity flow deposits – Classification, origin and significance. *Mar. Pet. Geol.*, **26**, 1900–1918.
Haughton, P.D.W., **Barker, S.P.** and **McCaffrey, W.D.** (2003) "Linked" debrites in sand-rich turbidite systems - Origin and significance. *Sedimentology*, **50**, 459–482.
Hirayama, J. and **Nakajima, T.** (1977) Analytical study of turbidites, Otadai Formation, Boso Peninsula, Japan. *Sedimentology*, **24**, 747–779.
Hiscott, R.N. (1981) Deep-sea fan deposits in the Macigno Formation (Middle-Upper Oligocene) of the Gordana Valley, northern Apennines, Italy: Discussion.
Howell, J.A., **Schwarz, E.**, **Spalletti, L.A.** and **Veiga, G.D.** (2005) The Neuquén Basin: an overview. *Geol. Soc. London, Spec. Publ.*, **252**, 1–14.
Jobe, Z.R., **Lowe, D.R.** and **Morris, W.R.** (2012) Climbing-ripple successions in turbidite systems: Depositional environments, sedimentation rates and accumulation times. *Sedimentology*, **59**, 867–898.
Joseph, P., **Babonneau, N.**, **Bourgeois, A.**, **Cotteret, G.**, **Eschard, R.**, **Garin, B.**, **Gomes De Souza, O.**, **Granjeon, D.**, **Guillocheau, F.** and **Lerat, O.** (2000) The Annot Sandstone outcrops (French Alps): architecture description as input for quantification and 3D reservoir modeling. In: *P. Weimer, RM Slatt, J. Coleman, NC Rosen, H. Nelson, AH Bouma, MJ Styzen, and DT Lawrence, Deep-Water Reservoirs of the World: Gulf Coast Section SEPM Foundation 20th Annual Research Conference, SEPM CD Special Publication*, 28, 422–449.
Kane, I.A. and **Pontén, A.S.M.** (2012) Submarine transitional flow deposits in the Paleogene Gulf of Mexico. *Geology*, **40**, 1119–1122.
Kenyon, N.H., **Klaucke, I.**, **Millington, J.** and **Ivanov, M.K.** (2002) Sandy submarine canyon-mouth lobes on the western margin of Corsica and Sardinia, Mediterranean Sea. *Mar. Geol.*, **184**, 69–84.
Koo, W.M., **Olariu, C.**, **Steel, R.J.**, **Olariu, M.I.**, **Carvajal, C.R.** and **Kim, W.** (2016) Coupling Between Shelf-Edge Architecture and Submarine-Fan Growth Style In A Supply-Dominated Margin. *J. Sediment. Res.*, **86**, 613–628.
Kostrewa, R. (2004) Internal Architecture, Geometry and Reservoir Characterisation of Depositional Lobes in Outcrop and Subsurface: Examples from S-Turkey and the North Sea.
Law, B.E. (2002) Basin-centered gas systems. *Am. Assoc. Pet. Geol. Bull.*, **86**, 1891–1919.
Legarreta, L. and **Gulisano, C.A.** (1989) Análisis estratigráfico secuencial de la Cuenca Neuquina (Triásico superior-Terciario inferior). In: *Cuencas sedimentarias argentinas, Universidad Nacional de Tucumán San Miguel de Tucumán*, 6, 221–243.
Legarreta, L. and **Uliana, M.A.** (1991) Jurassic–Cretaceous marine oscillations and geometry of backarc basin fill, central Argentine Andes. *Int. Assoc. Sedimentol.*, **12**, 429–450.
Legarreta, L. and **Uliana, M.A.** (1996) The Jurassic succession in west-central Argentina: Stratal patterns, sequences and paleogeographic evolution. *Palaeogeogr. Palaeoclimatol. Palaeoecol.*, **120**, 303–330.
Legarreta, L., **ViIIar, H.J.**, **Cruz, C.E.**, **Laffitte, G.A.** and **Varadé, R.** (2008) Revisión integrada de los sistemas generadores, estilos de migración-entrampamiento y volumetría de hidrocarburos en los distritos productivos de la Cuenca Neuquina, Argentina. In: *VII*

Congreso de Exploración y Desarrollo de Hidrocarburos (Simposio de Sistemas Petroleros de las Cuencas Andinas),

Link, M.H. and **Nilsen, T.H.** (1980) The Rocks Sandstone, an Eocene sand-rich deep-sea fan deposit, northern Santa Lucia Range, California. *J. Sediment. Res.*, **50**, 583–601.

Lomas, S.A. and **Joseph, P.** (2004) Confined turbidite systems. *Geol. Soc. London, Spec. Publ.*, **222**, 1–7.

Lowe, D.R. (1982) Sediment gravity flows; II, Depositional models with special reference to the deposits of high-density turbidity currents. *J. Sediment. Res.*, **52**, 279–297.

Macdonald, H.A., **Peakall, J.**, **Wignall, P.B.** and **Best, J.** (2011) Sedimentation in deep-sea lobe-elements: implications for the origin of thickening-upward sequences. *J. Geol. Soc. London.*, **168**, 319–332.

Marini, M., **Milli, S.** and **Moscatelli, M.** (2011) Facies and architecture of the Lower Messinian turbidite lobe complexes from the Laga Basin (central Apennines, Italy). *J. Mediterr. Earth Sci.*, **3**, 45–72.

Marini, M., **Milli, S.**, **Ravnås, R.** and **Moscatelli, M.** (2015) A comparative study of confined vs. semi-confined turbidite lobes from the Lower Messinian Laga Basin (Central Apennines, Italy): Implications for assessment of reservoir architecture. *Mar. Pet. Geol.*, **63**, 142–165.

Maury, M.F. (1855) The pusical geography of the sea. 274 pp.

Menard, H.W. (1955) Deep-Sea Channels, Topography, and Sedimentation. *Am. Assoc. Pet. Geol. Bull.*, **39**, 236–255.

Middleton, G. V. and **Hampton, M.A.** (1973) S.E.P.M. Pacific Section Short Course Notes Part I Sediment gravitiy flows: mechanics of flow and deposition. *Turbid. Deep Water Sediment.*, 1–38.

Mohrig, D., **Ellis, C.**, **Parker, G.**, **Whipple, K.X.** and **Hondzo, M.** (1998) Hydroplaning of subaqueous debris flows. *Geol. Soc. Am. Bull.*, **110**, 387–394.

Morabito, G. (2010) Tesis Doctoral Tectónica y estructura del retroarco andino entre los 38 ° 15 ’ y los 40 ° S.

Mulder, T. and **Alexander, J.** (2001) The physical character of subaqueous density flows and their deposits. *Sedimentology*, **48**, 269–299.

Mulder, T. and **Etienne, S.** (2010) Lobes in deep-sea turbidite systems: State of the art. *Sediment. Geol.*, **229**, 75–80.

Mulder, T., **Syvitski, J.P.M.**, **Migeon, S.**, **Faugères, J.C.** and **Savoye, B.** (2003) Marine hyperpycnal flows: Initiation, behaviorand related deposits. A review. *Mar. Pet. Geol.*, **20**, 861–882.

Mutti, E. (1985) Turbidite Systems and Their Relations to Depositional Sequences. In: *Provenance of Arenites* (Ed. G.G. Zuffa), *Springer Netherlands*, Dordrecht, 65–93.

Mutti, E. (1992) Turbidite sandstones. *Agip, Istituto di geologia, Università di Parma*.

Mutti, E. (1974) Examples of ancient deep-sea fan deposits from circum-Mediterranean geosynclines.

Mutti, E., **Bernoulli, D.**, **Lucchi, F.R.** and **Tinterri, R.** (2009) Turbidites and turbidity currents from alpine “flysch” to the exploration of continental margins. *Sedimentology*, **56**, 267–318.

Mutti, E. and **Normark, W.R.** (1987) Comparing examples of modern and ancient turbidite systems: problems and concepts. In: *Marine clastic sedimentology*, *Springer*, 1–38.

Mutti, E. and **Normark, W.R.** (1991) An Integrated Approach to the Study of Turbidite Systems. In: *Seismic Facies and Sedimentary Processes of Submarine Fans and Turbidite*

Systems (Ed. P. Weimer and M.H. Link), *Springer New York*, New York, NY, 75–106.

Mutti, E., **Tinterri, R.**, **Benevelli, G.**, **Biase, D. di** and **Cavanna, G.** (2003) Deltaic, mixed and turbidite sedimentation of ancient foreland basins. *Mar. Pet. Geol.*, **20**, 733–755.

Normark, W.R., **Piper, D.J.W.** and **Hess, G.R.** (1979) Distributary channels, sand lobes, and mesotopography of Navy Submarine Fan, California Borderland, with applications to ancient fan sediments. *Deep. Turbid. Syst.*, 400.

Normark, W.R., **Piper, D.J.W.** and **Sliter, R.** (2006) Sea-level and tectonic control of middle to late Pleistocene turbidite systems in Santa Monica Basin, offshore California. *Sedimentology*, **53**, 867–897.

Olariu, C., **Steel, R.J.**, **Vann, N.**, **Tudor, E.P.**, **Shin, M.**, **Rene, W.**, **Gan, Y.P.**, **Jung, E.**, **De Almeida, F.**, **Giacomone, G.**, **Minisini, D.**, **Brinkworth, W.**, **Loss, M.L.**, **Iñigo, J.** and **Gutierrez, R.** (2019) CRITERIA FOR RECOGNITION OF SHELF-SLOPE CLINOFORMS USING OUTCROP DATA; JURASSIC LAJAS AND LOS MOLLES FORMATIONS, S. NEUQUEN BASIN, ARGENTINA.

Omil, R.G. and **Borghi, P.** (2017) EL GRUPO CUYO EN LA CUENCA NEUQUINA (ENGOLFAMIENTO Y DORSAL DE HUINCUL). MODELO SEDIMENTARIO ...

Paim, P.S.G., **Lavina, E.L.C.**, **Faccini, U.F.**, **da Silveira, A.S.**, **Leanza, H.** and **D'Avila, R.S.F.** (2011) Fluvial-derived turbidites in the Los Molles Formation (Jurassic of the Neuque´n Basin): Initiation, transport, and deposition. *Sediment Transf. from shelf to Deep water—Revisiting Deliv. Syst. AAPG Stud. Geol. 61*, 95–116.

Paim, P.S.G., **Silveira, A.S.**, **Lavina, E.L.C.**, **Faccini, U.F.**, **Leanza, H.A.**, **Teixeira De Oliveira, J.M.M.** and **D'Avila, R.S.F.** (2008) High resolution stratigraphy and gravity flow deposits in the Los Molles Formation (Cuyo Group - Jurassic) at La Jardinera region, Neuquén basin TT - Estratigrafía de alta resolución de depósitos de flujos gravitacionales de la Formación Los Molles (Grup. *Rev. la Asoc. Geológica Argentina*, **63**, 728–753.

Pichevin, L., **Mulder, T.**, **Savoye, B.**, **Gervais, A.**, **Cremer, M.** and **Piper, D.J.W.** (2003) The Golo submarine turbidite system (east Corsica margin): Morphology and processes of terrace formation from high-resolution seismic reflection profiles. *Geo-Marine Lett.*, **23**, 117–124.

Pickering, K.T. (1981) Two Types of Outer Fan Lobe Sequence, from the Late Precambrian Kongsfjord Formation Submarine Fan, Finnmark, North Norway. SEPM J Sediment Res. doi: 10.1306/212F7E87-2B24-11D7-8648000102C1865D

Pickering, K.T. and **Hiscott, R.N.** (1985) Contained (reflected) turbidity currents from the Middle Ordovician Cloridorme Formation, Quebec, Canada: an alternative to the antidune hypothesis. *Sedimentology*, **32**, 373–394.

Piper, D.J.W. and **Normark, W.R.** (1983) Turbidite depositional patterns and flow characteristics, Navy submarine fan, California Borderland. *Sedimentology*, **30**, 681–694.

Prélat, A. and **Hodgson, D.M.** (2013) The full range of turbidite bed thickness patterns in submarine lobes: controls and implications. *J. Geol. Soc. London.*, **170**, 209–214.

Prélat, A., **Hodgson, D.M.** and **Flint, S.S.** (2009) Evolution, architecture and hierarchy of distributary deep-water deposits: a high-resolution outcrop investigation from the Permian Karoo Basin, South Africa. *Sedimentology*, **56**, 2132–2154.

Raggio, M.F., **G., L.P.**, **F., S.** and **M., A.** (2014) Modelo de gas de Centro de Cuenca (Basin–Centered Gas System) en la Formaciòn Lajas. Un desafio exploratorio no convencional en el ambito del engolfamiento Neuquino. In: *Un desafio exploratorio No Convencional en el*

àmbito del Engolfamiento Neuquino. IX Congreso de Exploraciòn y Desarrollo de Hidrocarburos Simposio de Recursos No Convencionales, 163–185.

Ramos, V.A. (1998) Estructura del sector occidental de la faja plegada y corrida del Agrio, cuenca Neuquina, Argentina. *Congr. Latinoam. Geol.*, **10**, 105–110.

Reading, H.G. and **Richards, M.** (1994) Turbidite systems in deep-water basin margins classi ed by grain size and feeder system. American Association of. *Pet. Geol. Bull.*, **78**, 792–822.

Ricci Lucchi, F. (1975) Depositional cycles in two turbidite formations of northern Apennines (Italy). *J. Sediment. Petrol.*, **45**, 3–43.

Rozman, D.J., **Bouma, A.H.** and **Stone, C.G.** (2000) Characterization of a fine-grained outer submarine fan deposit, Tanqua-Karoo Basin, South Africa. *Spec. Publ.*, **68**, 279–290.

Satur, N., **Hurst, A.**, **Cronin, B.T.**, **Kelling, G.** and **Gürbüz, K.** (2000) Sand body geometry in a sand-rich, deep-water clastic system, Miocene Cingoz Formation of southern Turkey. *Mar. Pet. Geol.*, **17**, 239–252.

Shin, M. (2015) Architecture of coarse grained (conglomeratic) deep water lobes at the base of a sandstone dominated fan, Jurassic Los Molles Formation, Neuquen Basin, Argentina. 116.

Sinclair, H.D. (1994) The influence of lateral basinal slopes on turbidite sedimentation in the Annot sandstones of SE France. *J. Sediment. Res.*, **64**, 42–54.

Sinclair, H.D. and **Cowie, P.A.** (2003) Basin-Floor Topography and the Scaling of Turbidites. *J. Geol.*, **111**, 277–299.

Sinclair, H.D. and **Tomasso, M.** (2002) Depositional Evolution of Confined Turbidite Basins. *J. Sediment. Res.*, **72**, 451–456.

Smith, R. (2004) Turbidite systems influenced by structurally induced topography in the multi-sourced Welsh Basin. *Geol. Soc. London, Spec. Publ.*, **222**, 209–228.

Sohn, Y.K. (1997) On traction-carpet sedimentation. *J. Sediment. Res.*, **67**, 502–509.

Southard, J.B. (1991) Experimental determination of bed-form stability. *Annu. Rev. Earth Planet. Sci.*, **19**, 423–455.

Southern, S.J., **Kane, I.A.**, **Warchoł, M.J.**, **Porten, K.W.** and **McCaffrey, W.D.** (2017) Hybrid event beds dominated by transitional-flow facies: Character, distribution and significance in the maastrichtian springar formation, north-west vøring basin, Norwegian Sea. *Sedimentology*, **64**, 747–776.

Southern, S.J., **Patacci, M.**, **Felletti, F.** and **McCaffrey, W.D.** (2015) Influence of flow containment and substrate entrainment upon sandy hybrid event beds containing a co-genetic mud-clast-rich division. *Sediment. Geol.*, **321**, 105–122.

Spychala, Y.T., **Hodgson, D.M.**, **Prélat, A.**, **Kane, I.A.**, **Flint, S.S.** and **Mountney, N.P.** (2017) Frontal and Lateral Submarine Lobe Fringes: Comparing Sedimentary Facies, Architecture and Flow Processes. *J. Sediment. Res.*, **87**, 75–96.

Sumner, E.J., **Amy, L.A.** and **Talling, P.J.** (2008) Deposit Structure and Processes of Sand Deposition from Decelerating Sediment Suspensions. *J. Sediment. Res.*, **78**, 529–547.

Sumner, E.J., **Talling, P.J.** and **Amy, L.A.** (2009) Deposits of flows transitional between turbidity current and debris flow. *Geology*, **37**, 991–994.

Talling, P.J. (2001) On the frequency distribution of turbidite thickness. *Sedimentology*, **48**, 1297–1329.

Talling, P.J., **Amy, L.A.** and **Wynn, R.B.** (2007) New insight into the evolution of large-volume turbidity currents: Comparison of turbidite shape and previous modelling results. *Sedimentology*, **54**, 737–769.

Talling, P.J., **Masson, D.G.**, **Sumner, E.J.** and **Malgesini, G.** (2012) Subaqueous sediment

density flows: Depositional processes and deposit types. *Sedimentology*, **59**, 1937–2003.
Tinterri, R. and **Piazza, A.** (2018) Turbidites facies response to the morphological confinement of a foredeep (Cervarola Sandstones Formation, Miocene, northern Apennines, Italy). Sedimentology. doi: 10.1111/sed.12501
Tokuhashi, S. (1989) Two stages of submarine fan sedimentation in an ancient forearc basin, central Japan. *Sediment. facies Act. plate margin*, 439–468.
Tudor, E.P. (2014) Approved By Supervising Committee. Thesis Rep. doi: 10.1096/fj.15-282475
van der Werff, W. and **Johnson, S.D.** (2003) Deep-sea fan pinch-out geometries and their relationship to fan architecture, Tanqua Karoo basin (South Africa). *Int. J. Earth Sci.*, **92**, 728–742.
Vann, N., **Olariu, C.** and **Steel, R.** (2014) I : Slope to Basin-floor Evolution of Channels to Lobes , Jurassic Los Molles Formation , Neuquén Basin , Argentina. doi: 10.1016/j.synthmet.2011.04.008
Vergani, G.D. (2005) Control estructural de la sedimentación jurásica (Grupo Cuyo) en la Dorsal de Huincul, cuenca Neuquina, Argentina. Modelo de falla lístrica rampa-plano, invertida. *Boletín Inf. Pet.*, **1**, 32–42.
Vergani, G.D., **J., T.A.**, **Belloti, H.J.** and **Welsink, H.J.** (1995) Tectonic Evolution and Paleogeography of the Neuquen Basin, Argentina: ABSTRACT. *Am. Assoc. Pet. Geol. Bull.*, **79**, 383–402.
Villar, H.J., **Legarreta, L.**, **Cruz, C.E.**, **Laffitte, G.** and **Vergani, G.** (2005) Los Cinco Sistemas Petroleros Coexistentes En El Sector Sudeste De La Cuenca Neuquina: Definición Geoquímica Y Comparación a Lo Largo De Una Transecta De 150 Km. *VI Congr. Explor. y Desarro. Hidrocarburos, Mar Plata*, 1–17.
Vrolijk, P.J. and **Southard, J.B.** (1997) Experiments on rapid deposition of sand from high-velocity flows.
Walker, R.G. and **Mutti, E.** (1973) Turbidite facies and facies associations. *Turbid. Deep water Sediment.*, 119–158.
William R. Normark (2) (1978) Fan Valleys, Channels, and Depositional Lobes on Modern Submarine Fans: Characters for Recognition of Sandy Turbidite Environments. *Am. Assoc. Pet. Geol. Bull.*, **62**, 912–931.
Wood, A. and **Smith, A.J.** (1957) The sedimentation and sedimentary history of the Aberystwyth Grits (Upper Llandoverian). Q. J. Geol. Soc. 114:163–195.
Yrigoyen, M.R. (1991) Hydrocarbon resources of Argentina. *Petrotecnia*, **13**, 38–54.
Zavala, C., **Arcuri, M.**, **Meglio, M. Di**, **Diaz, H.G.** and **Contreras, C.** (2011) A Genetic Facies Tract for the Analysis of Sustained Hyperpycnal Flow Deposits. *Sediment Transf. from shelf to Deep water—Revisiting Deliv. Syst. AAPG Stud. Geol. 61*, 31–52.